ORNL/TM-2019/1372

RAPID: The Development and Application of a Hybrid High Pressure Ion Chromatography and Inductively Coupled Plasma Mass Spectrometry Method for the Direct Analysis of Irradiated Materials

B. D. Roach
E. K. Fenske
D. C. Glasgow
R. H. Ilgner
T. J. Keever
C. R. Hexel
J. M. Giaquinto

December 2019

OAK RIDGE NATIONAL LABORATORY
MANAGED BY UT-BATTELLE FOR THE US DEPARTMENT OF ENERGY

Nuclear Analytical Chemical and Isotopics Laboratories
Chemical Sciences Division

RAPID: THE DEVELOPMENT AND APPLICATION OF A HYBRID HIGH PRESSURE ION CHROMATOGRAPHY AND INDUCTIVELY COUPLED PLASMA MASS SPECTROMETRY SYSTEM FOR THE ANALYSIS OF IRRADIATED MATERIALS

B. D. Roach, E. K. Fenske, D. C. Glasgow, R. H. Ilgner,
T. J. Keever, C. R. Hexel, J. M. Giaquinto

Date Published: December 2019

Prepared by
OAK RIDGE NATIONAL LABORATORY
Oak Ridge, TN 37831-6283
managed by
UT-BATTELLE, LLC
for the
US DEPARTMENT OF ENERGY
under contract DE-AC05-00OR22725

EXECUTIVE SUMMARY

RAPID (Rapid Analysis of Post-Irradiation Debris) is an automated online separation–direct analysis method developed at Oak Ridge National Laboratory (ORNL) to measure both radioactive and stable fission isotopes by mass. Developed to measure the concentration and isotopic composition of over 40 elements down to the femtogram level, RAPID demonstrates the sensitivity, stability, and precision required to achieve accurate, low-level analyses of elements of non-natural origin. The application of the RAPID method to silica- and soil-based matrices achieved complete matrix exclusion and direct online analysis of the elementally separated analytes, yielding precise isotopic compositions. When combined with isotope dilution, this approach yielded elemental concentrations with low uncertainties, providing a rapid analytical method that encompasses group I and II metals, transition metals, refractory metals, platinum group metals, lanthanides, and actinides. The robustness, sensitivity, reproducibility, and numerous applications to a number of fields in nuclear measurements have been confirmed.

1. INTRODUCTION

Anthropogenic nuclear activities, such as nuclear weapons testing, nuclear fuel cycle operations, medical isotope production, and actinide production, produce significant quantities of materials with trace elemental impurities of non-natural isotopic abundance. The precise and timely analysis of trace levels of fission isotopes in irradiated materials is key to a number of research and development areas in the nuclear field, specifically for modeling and simulation validation, nuclear forensics, and isotope production [1, 2]. The analysis of the short-lived, long-lived, and stable fission isotopes resulting from a nuclear event is critical in the forensic attribution process that will follow [3]. The improvement of modeling capabilities also occurs through the verification of fission products formed during reactor operation [4–8] and material irradiation [9, 10]. ^{235}U thermal fission products, being very well characterized, vary from stable isotopes to numerous short- and long-lived isotopes [11, 12], thus, both radiometric and mass-based analyses are traditionally utilized for full characterization. To adequately and efficiently characterize the short-lived isotopes at the same time as the longer-lived and stable isotopes, an inclusive, rapid analytical method is desired.

Due to the limited sample size, the analytical tools traditionally employed for fission product analysis are radio-analytical techniques, such as non-destructive gamma-ray spectroscopy [13–15], and neutron activation analysis [16]. Unfortunately, in such samples, spectral interferences and the need for background discrimination increase dramatically the closer to the time of irradiation the analysis occurs. Either a cooling-period must be observed, to allow for shorter lived isotopes to decay, or the results will be subject to increased uncertainties and detection limits [17, 18]. ^{135}Cs, ^{90}Sr, and ^{147}Pm are prime examples of important fission-generated analytes that suffer from both signal suppression and significant interferences using traditional radiochemical techniques and currently cannot be directly detected without significant, and lengthy, chemical separations [19].

Ion chromatography (IC) has traditionally been used for the separations of actinide and fission products prior to their analysis since the 1980's – it is a versatile, sensitive, yet lengthy technique for the determination of various cations and anions at ultra-trace levels. IC, when coupled with an inductively coupled plasma mass spectrometer (ICPMS), separates and subsequently detects trace-level quantities of elements from various matrices, such as environmental samples, nuclear waste, uranium ore, and more. Almon [20] et al. introduced the procedure of analyzing fission products and actinides in nuclear waste using IC-ICPMS beginning in 1991; similarly, in 1997, Betti [21] utilized IC-ICPMS for additional analysis of fission products and actinides in high-level nuclear waste, as well as spent nuclear fuel. In the early

2000's, IC-ICPMS methods were developed to analyze actinides, lanthanides, and other metals in samples such as "urban road dust" and atmospheric particles [22], National Institute of Standards and Technology (NIST) standards of soil and a human lung [23], environmental samples [24, 25], uranium materials [26], and spent nuclear fuel [27–30]. More recently, work has been done to isolate and determine the concentrations of elements such as Np [31], Mg [32], Sr [33, 34], Cs [35], Pu [36, 37], Nd [38], Bk/Cf [39], Sm [40], and various other metals [41, 42] through IC-ICPMS analysis.

Isotope dilution (ID) is a method of determining analyte concentration in which certified isotopically enriched standards are gravimetrically added to the sample being analyzed [43, 44]. Using the isotopic composition of the sample and the isotopically diluted sample, the concentration of the analyte can be determined with uncertainties in the 1-2% range [45]. ID is a powerful technique that employs an internal calibrant, which has distinct advantages over an external calibration technique, especially when the analyte in question is present in small amounts and in the presence of a complex matrix.

High-pressure ion chromatography (HPIC) coupled with ID, using ICPMS for isotopic analysis, was recently employed in improvements to commercial reactor depletion codes for mixed oxide (MOX) fuels irradiated in U.S. reactors [4, 46]. Utilizing this methodology, key rare earth and cesium fission products were measured in irradiated MOX fuels for the Department of Energy (DOE) Fissile Materials Disposition Program (FMDP) Office project, proving the feasibility for the repurposing of weapons grade plutonium through use as a nuclear fuel [47].

The focus of this work can be split into two distinct sections, the first being the development, validation, and qualification, of RAPID (Rapid Analysis of Post-Irradiation Debris), an analytical technique using a hyphenated HPIC-ICPMS method to yield precise isotopic compositions and, by combination with isotope dilution, elemental concentrations down to the low picogram level. This section will also encompass the development of matrix exclusion via modification of HPIC separation prior to analysis by ICPMS which resulted in both separation of isobaric-, and polyatomic-interferences, from the isotopes of interest. Development of the eluent separation scheme, the method stability and isotopic detection limits together with the accuracy of measured isotope ratios has been investigated. Together with the development of the RAPID method, the results of its application in combination with ID to samples in a synthetic soil matrix as well as NIST certified SRM-2711a Montana II soil standard, will be presented.

The second section of this work had the goal to achieve measurements of non-natural isotopic signatures at concentrations ranging from those in spent fuels to those likely present in post-detonation material [48, 49],

thus this study presents the analysis of a highly-enriched uranium (HEU) target irradiated to yield ~10^{14} fissions. With the initial analysis occurring less than 200 h post-irradiation and requiring less than one hour per sample, multiple analyses over a six-week period enabled the measurement of shifting isotopic compositions of nine key fission elements, namely, Ce, Sr, Y, La, Ce, Pr, Nd, Pm, and Sm. The isotopic concentrations were subsequently determined via both RAPID and ICPMS using NIST-traceable natural standards, and high-purity germanium (HPGe) gamma detectors were utilized to confirm the determined concentrations of several short-lived fission isotopes. The determined isotopic abundances and concentrations are presented in terms of precision and accuracy when compared to those predicted by the ORIGEN modeling software.

2. MATERIAL AND METHODS

2.1 INSTRUMENTATION

The equipment employed was a Thermo Scientific™ Dionex™ ICS-5000+ HPIC system coupled to a Thermo Scientific iCAP™ Q quadrupole ICPMS. The HPIC system is comprised of an AS-AP autosampler, complete with sample dilution and fraction collection capabilities, a gradient mixing pump capable of combining four different eluents in the same analysis, and a thermal compartment containing the injection loop and separation column, able to maintain temperatures 5–85 ºC for constant elution times and reproducibility.

The ICPMS is equipped with a wide range sensitivity detector (from mg/L to pg/L), a robust torch capable of withstanding the introduction of salts and organic matter from the HPIC eluents, a wide bore (high salt) nebulizer which can nebulize solutions of higher density and organic content, and a specialized collision cell which reduces the signal-to-noise ratio for high precision measurements of low mass analytes.
Chromatographic separation was performed using a metal-free HPIC pump ICS 5000 (ThermoFisher Scientific), an injection valve, an IonPac CG5A guard column, and an IonPac CS5A column. These columns were chosen as they have both cation and anion exchange capabilities, containing both sulfonic acid and alkanol quaternary ammonium functional groups. The analytical column was connected to the nebulizer of the ICPMS instrument using 20-cm-long PEEK tubing via a mixing T-piece, which both re-acidified the sample post-column and provided an internal standard to monitor signal stability. The iCAP was fitted with a cyclonic quartz spray chamber, a nickel sampler cone, and a nickel skimmer cone with a standard skimmer insert. A pre-defined daily QC performance report was used to ensure optimized iCAP

operating conditions. Data were processed using Thermo Fisher Scientific Qtegra software **Table 1** summarizes the experimental and operating conditions of the HPIC-ICPMS system.

Table 1. Experimental and operating conditions of the HIPC-ICPMS system.

Thermo Scientific Dionex ICS-5000+ HPIC	
PEEK injection loop	25 µL
IonPac CG5A column	50 x 4 mm i.d.
IonPac CS5A column	250 x 4 mm i.d.
	Substrate 9 µm particles
	40 µequivalents/column
Eluent flow rate	1.0 mL. min^{-1}
System pressure at 1.0 mL. min^{-1}	~1600 psi
Post-column internal standard flow rate	0.1 mL. min^{-1}
PEEK HPIC-ICPMS connection tubing	0.25 mm i.d.
Thermo Scientific iCAP Q quadrupole ICPMS	
Sampler cone diameter	1.1 mm
Skimmer cone diameter	0.5 mm
Plasma power	1549 W
Interface temperature	35.0C
Nebulizer gas flow rate	1.0 L. min^{-1}
Axillary gas flow rate	0.78 L. min^{-1}
Cool gas flow rate	13.95 L. min^{-1}

2.2 REAGENTS AND STANDARDS

Eluents for HPIC and all other solutions were prepared with trace metals basis grade chemicals and ultra-pure water (18.2 MΩ cm) from a Millipore Milli-Q™ water purification system. Chemicals for eluents include: diglycolic acid (DGA, $C_4H_6O_5$) (recrystallized) (>98%, lot A0353334) (Acros Organics, New Jersey, USA), 2,6-pyridinedicarboxylic acid (PDCA, $C_7H_5NO_4$) (99.999% metals basis lot BCBQ3850V) (Fluka, Sigma-Aldrich Co.), glacial acetic acid ($C_2H_4O_2$) (99.99% trace metals basis lot SHBH2511V) (Sigma-Aldrich Co., 3050 Spruce Street, St. Louis, MO 63103 USA), oxalic acid

($C_2H_2O_4$) (99.999% trace metals basis lot MKCC3466) (Sigma-Aldrich Co.). These were dissolved in ultra-pure water, then buffered with ammonium hydroxide (NH_4OH) (20-22% as NH_3) (trace metal grade lot 7115080) (Fisher Scientific, 1 Reagent Lane, Fair Lawn, NJ 07410), to a final pH of 4.5 - 4.8.

Working standard solutions were prepared for HPIC-ICPMS analyses in 5% nitric acid (HNO_3) by diluting the stock standard solutions in ultra-pure water: IV-ICPMS-71A (10 mg L^{-1}) (Lot K2-MEB631044), IV-ICPMS-71B (10 mg L^{-1}) (Lot K2-MEB603127), and IV-ICPMS-71D (10 mg L^{-1}) (Lot K2-MEB631034) (Inorganic Ventures, 300 Technology Dr., Christiansburg, VA 24073 USA, see **Table 2**) and spiking with an in-house mixed actinide standard from various sources. During IDMS quantifications, samples were spiked with enriched isotope standard IDMS-023 (stable isotope mixture: ^{150}Nd, ^{151}Eu, ^{152}Sm, and ^{155}Gd, 11.1, 0.331, 3.49, and 0.358 µg g^{-1} respectively) (Isotope Business Office, ORNL, 1 Bethel Valley Road, Oak Ridge, TN 37831).

Table 2. NIST tracible standards and their elemental components

Element	Standard
Barium	IV-ICPMS-71-A
Arsenic	IV-ICPMS-71-A
Iridium	IV-ICPMS-71-C
Selenium	IV-ICPMS-71-A
Ruthenium	IV-ICPMS-71-A
Tellurium	IV-ICPMS-71-B
Scandium	IV-ICPMS-71-D
Neptunium	NIST SRM-4241a
Niobium	IV-ICPMS-71-B
Lithium	IV-ICPMS-71-D
Osmium	IV-ICPMS-71-C
Rubidium	IV-ICPMS-71-A
Cesium	IV-ICPMS-71-A
Thallium	IV-ICPMS-71-A
Tin	IV-ICPMS-71-B

Titanium	IV-ICPMS-71-B
Gallium	IV-ICPMS-71-A
Rhodium	IV-ICPMS-71-C
Iron	IV-ICPMS-71-A
Lead	IV-ICPMS-71-A
Zinc	IV-ICPMS-71-A
Copper	IV-ICPMS-71-A
Palladium	IV-ICPMS-71-C
Strontium	IV-ICPMS-71-A
Nickel	IV-ICPMS-71-A
Cobalt	IV-ICPMS-71-A
Cadmium	IV-ICPMS-71-A
Gold	IV-ICPMS-71-C
Tantalum	IV-ICPMS-71-B
Manganese	IV-ICPMS-71-A
Antimony	IV-ICPMS-71-B
Lanthanum	IV-ICPMS-71-A
Cerium	IV-ICPMS-71-A
Praseodymium	IV-ICPMS-71-A
Germanium	IV-ICPMS-71-B
Neodymium	IV-ICPMS-71-A
Samarium	IV-ICPMS-71-A
Europium	IV-ICPMS-71-A
Gadolinium	IV-ICPMS-71-A
Terbium	IV-ICPMS-71-D
Curium	ORNL-WRM-Cm
Americium	ORNL-WRM-Am
Dysprosium	IV-ICPMS-71-A
Yttrium	IV-ICPMS-71-D

Holmium	IV-ICPMS-71-A
Plutonium	IRMM-86
Thorium	IV-ICPMS-71-A
Thulium	IV-ICPMS-71-A
Zirconium	IV-ICPMS-71-B

Preparation of a trace metal grade surrogate soil matrix was carried out via mixing of the following trace pure chemicals: silicon dioxide (SiO_2) (99.998% trace metal basis lot A0357680) (Acros Organics); calcium hydroxide ($Ca(OH)_2$) (99.995% trace metals basis lot MKBC4261); iron (III) oxide (Fe_2O_3) (>99.995% trace metals basis lot MKCC0460); magnesium nitrate hexahydrate ($Mg(NO_3)_2 \cdot 6H_2O$) (99.999% trace metals basis lot MKBZ9637V); and aluminum nitrate nonahydrate ($Al(NO_3)_3 \cdot 9H_2O$) (99.997% trace metals basis lot MKBZ3362V) (Sigma-Aldrich Co.). These were weighed out in proportions to simulate the NIST SRM 2711a soil standard, although the elemental concentrations per gram surrogate are approximately half of those found in SRM 2711a.

The HEU target was prepared using the certified reference standard U930-D (93.2% ^{235}U, New Brunswick Laboratory, IL, USA). Working standard solutions were prepared for HPIC-ICPMS analyses in 5% nitric acid (HNO_3) by diluting the stock standard solutions in ultra-pure water: IV-ICPMS-71A (10 mg L^{-1}), IV-ICPMS-71B (10 mg L^{-1}), and IV-ICPMS-71D (10 mg L^{-1}) (Inorganic Ventures, VA, USA).

2.3 SURROGATE SOIL DIGESTION

Dissolution of the trace pure surrogate soil mixture was performed via microwave digestion using a Discover SP-D® (CEM Corporation Matthews, NC 28106). The digestion was carried out following a previously reported method [50]. *Ca.* 200 mg of the surrogate was placed in Teflon® lined Pyrex® pressure vessels and allowed to pickle overnight in nitric acid (HNO_3, 16 M, 2 ml, 67% v/v, Optima, Lot 1215030) and hydrofluoric acid (HF, 29M, 2 mL, 47-51% v/v, Optima, Lot 5213102). The surrogate was microwave digested under the conditions given in **Table 3**. After cooling to room temperature, HF (1mL, 29M, 47-51% v/v, Optima) was added. A second microwave digestion was then performed using the same conditions. 10mL of boric acid (H_3BO_3, 5%, 99.999% trace metals basis, Lot MKCC0193) was then added

to complex the excess HF and aid in the digestion of possible insoluble fluorides. After the boric acid addition, a third microwave digestion was then performed using the same conditions.

Table 3. Microwave digestion settings used for each digestion stage for the dissolution of the surrogate soil

Stage	Temp (°C)	Ramp Time (min)	Hold Time (min)	Pressure (PSI)	Power (W)	Stirring
1	100	5:00	00:10	450	250	Medium
2	175	5:00	00:10	450	300	Medium
3	180	5:00	00:10	450	300	Medium
4	180	10:00	00:10	450	300	Medium
5	175	5:00	00:10	450	300	Medium

2.4 NIST SRM2711A MONTANA SOIL DIGESTION

A NIST certified standard, SRM2711a Montana Soil, was analyzed for lanthanide content using IDMS coupled with the RAPID method. The SRM2711a soil (*ca.* 40 mg), dried for 2hr at 110 °C, and ORNL-024 enriched-isotope mixed-lanthanide standard (^{140}Ce, 131.3 ng/g; ^{150}Nd, 47.0 ng/g; ^{152}Sm, 12.4 ng/g; ^{151}Eu, 2.30ng/g; and ^{155}Gd, 4.16 ng/g; 4.8 mL, in 0.5N HNO_3, Optima) were combined by weight into a Teflon® (TFM) pressure vessel prior to dissolution. Dissolution of the spiked SRM2711a soil was performed via microwave digestion using a Milestone® HPR-1000 microwave (Milestone Inc., Shelton, CT), following an in-house digestion method for silica-based materials. Nitric acid (HNO_3, 8M, 10 ml, Optima), hydrochloric acid (HCl, ~10M, 2 ml, Optima) and hydrofluoric acid (HF, 29M, 0.4 mL, 47-51% v/v, Optima) were added by volume to the vessel containing the spiked SRM. The spiked SRM2711a soil was microwave digested under the conditions given in **Table 4**. After cooling to room temperature, a 5× dilution of the digest in nitric acid (HNO_3, 0.5 M, Optima) was used in the analysis.

Table 4. Microwave digestion settings used for the dissolution of the NIST SRM2711a Montana II soil standard

Time (min)	Power (W)	Temp (°C)
15	800	25 to 80
15	800	80
15	800	80 to 185
40	800	185

2.5 HEU IRRADIATION AND TARGET PREPARATION

The HEU target was prepared by evaporating portions of U930-D into a high-purity quartz ampoule, shown in **Figure 1**, resulting in a target containing ~80 μg ^{235}U. After flame-sealing under partial vacuum, the ampoule was counted on HPGe detectors to verify the fissile mass prior to irradiation.

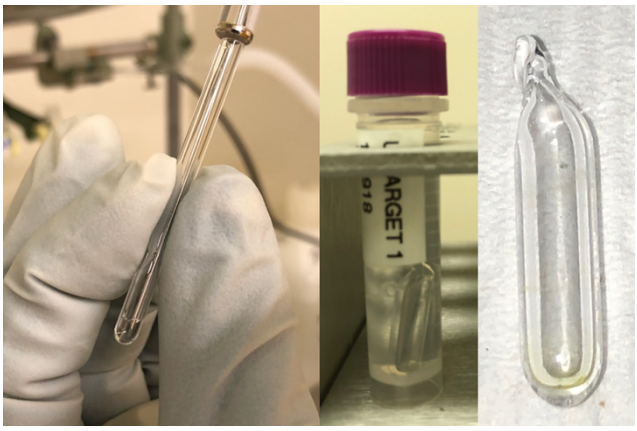

Figure 1. The micro-syringe loading of NBL CRM U930-D (right) into the quartz tube, and leaching (middle) of the vacuum sealed quartz target (left).

Following the guidance of the Los Alamos National Laboratory PAssive Non-Destructive Assay (PANDA) manual [51], the 185.7 keV gamma-ray was analyzed in background-subtracted spectra. An ORIGEN calculation resulted in an irradiation time required to reach 10^{14} fissions, ensuring enough fission

material is produced but minimizing the required cooling period post-irradiation. The target was irradiated at the Nuclear Analytical Chemical and Isotopics Laboratory (NACIL) Neutron Activation Analysis (NAA) laboratory, located within the High Flux Isotope Reactor (HFIR) facility. The thermal and epithermal flux populations were measured using dilute manganese and gold flux monitors, respectively. The thermal flux was 4.17×10^{14} and the epithermal measured 1.12×10^{13}, with both having units of neutrons cm^{-2} s^{-1}. For modeling purposes, the total flux over the broader neutron spectrum was calculated to be 6.57×10^{14} n cm^{-2} s^{-1}. The target was sealed in a graphite rabbit and irradiated for one hour. Post-irradiation and a 24 h cooling period, the dose rate of the unopened rabbit was measured. After a further cooling period, the irradiated target was shipped from the HFIR facility to another NACIL laboratory building for chemical processing and analysis. The received target was leached, while sealed, in 4M HNO_3, and tare weights in a Savillex vessel were determined. The target was opened by submersion in 4M HNO_3 (Optima) in a pre-leached, malleable polytetrafluoroethylene (PTFE) vessel under controlled crushing with a pre-cleaned mini-vice (**Figure 2**). The opened target was then quantitatively transferred back into the pre-tared leaching vessel for sealed heat leaching. The vessel was heat-leached at ~80°C for 4 h in HNO_3 (3 mL, 4M, Optima), allowed to cool, and the final weight was taken to determine solution weight and volume. Post-leaching, the uranium content was determined with isotope dilution mass spectrometry (IDMS) using a certified ^{238}U standard (IV-ICPMS-71A, Inorganic Ventures).

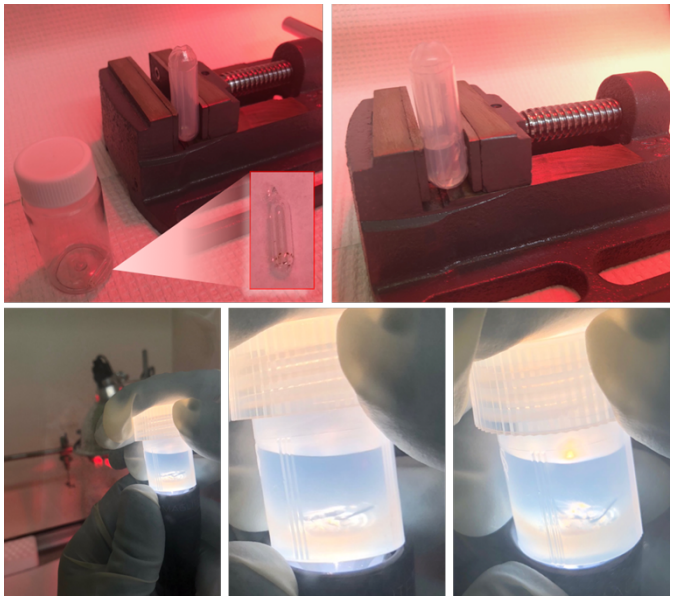

Figure 2. The setup for crushing and heat leaching of the irradiated HEU target featuring the pre-cleaned mini-vice, the double walled PTFE malleable vessel and the irradiated target (top) and the crushed target post-transfer, rinsing, and heat-leaching in a Savillex container (bottom)

2.6 SOFTWARE AND DATA PROCESSING

The SCALE code system [52], used internationally in support of spent nuclear fuel transportation and storage applications, includes an isotope depletion and decay analysis module known as ORIGEN [53]. The ORIGEN module was used to predict the changing isotopic masses of fission products in an irradiated HEU target over a six-week period. The model accurately reproduces the flux spectrum in the specific pneumatic tube used for irradiation in ORNL's neutron activation analysis (NAA) laboratory, enabling accurate prediction of total fissions in the target based on the mass of fissile material loaded. All measured isotopic data reported references the integrated isotopic peak areas in a transient signal as determined by the Thermo Fisher Scientific Qtegra software, using an *m/z* trace and a pre-determined elution time. Peak fitting and smoothing in the Qtegra software were applied post-acquisition, statistically reducing the observed uncertainties and enabling peak area comparisons between isotope peaks from the same element, yielding isotopic ratios in atom percent. The chromatographic peak fitting and smoothing settings applied to determine peak area, found within the "Peak Detection" settings of the Qtegra software, are as detailed previously [54–56]. The limits of detection (LOD) and quantitation (LOQ) for the individual isotopes were calculated using a linear regression slope analysis [57–60]. A series of multi-elemental standards with column loading ranging from 25 pg to 2.5 ng were analyzed utilizing the HPIC-ICPMS separation scheme. After the peak areas were determined using the Qtegra software, the data was exported to Excel and, employing the Analysis Toolpak, linear regression analysis was carried out using the regression function. This yielded, amongst other information, the standard deviation of the Y intercept from a least-squares linear regression slope analysis. For elements with multiple isotopes, the analyzed isotope was multiplied by the isotopic abundance to yield isotopic LOD and LOQ values, which will be important when employing enriched isotope standards for IDMS analyses. Additionally, fission product impact depths into the ampoule walls during irradiation were obtained with a software package focused on the stopping power and range into matter (SRIM), which calculates the range of variously-energized ions into targets using a quantum mechanical model of ion-atom collisions [61].

3. RESULTS AND DISCUSSION – SECTION I

3.1 DEVELOPED SEPARATION SCHEME

Existing separation schemes published by Dionex [62–64] were modified for ICPMS compatibility and investigated for several factors, including separation of analytes, peak shape produced in the chromatogram, salt content, and organic concentration. To establish a separation method maximizing the sample and minimizing the analysis time, a single separation scheme was established, combining PDCA, previously established for transition metal separation [64], and oxalic acid/DGA, which has been shown to efficiently separate the lanthanide elements [64]. The resulting analysis provided the isobaric separation and quantitation of 48 elements of interest in nuclear materials. **Table 5** details the gradient elution profile for the elemental separation with the four eluents being: deionized water, used mainly as a diluent for the other eluents; 6 mM PDCA (with 90 mM acetic acid, buffered to pH 4.5 with NH_4OH) used to separate transition metals, refractory metals, and group I and II metals; 100 mM oxalic acid (buffered to pH 4.8 with NH_4OH) and 100 mM DGA (buffered to pH 4.8 with NH_4OH), both used for lanthanide and actinide separation. The resulting separation scheme is analogous to that shown in **Figure 3**.

Table 5. Timings and percent contribution from each eluent for the separation scheme

Time (s)	Deionized H_2O (%)	PDCA (%)	DGA (%)	Oxalic Acid (%)
0	0	100	0	0
720	0	100	0	0
726	100	0	0	0
1020	40	0	0	60
1026	40	0	0	60
1260	40	0	0	60
1266	20	0	0	80
1800	51	0	23	26
2100	0	0	100	0
2700	100	0	0	0
2706	0	0	0	100
2820	0	0	0	100
2826	0	100	0	0

3120	0	100	0	0

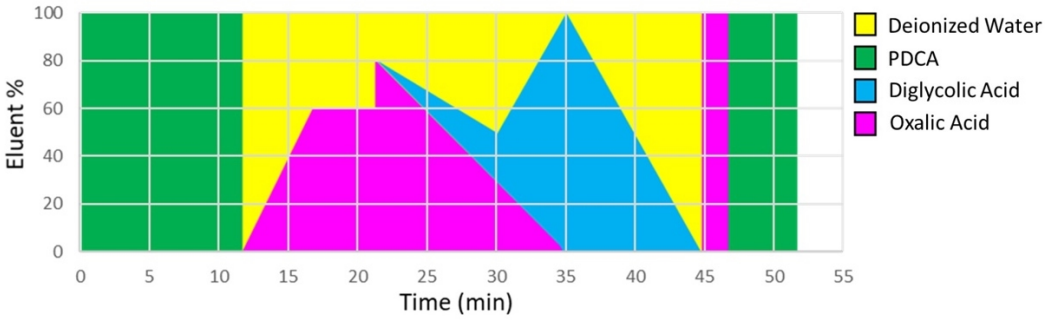

Figure 3. Gradient separation scheme using deionized water (yellow), 6 mM PDCA (green), 100 mM oxalic acid (pink), and 100 mM DGA (blue).

Post-separation, a two-minute washing period of 100% oxalic acid, followed by a five-minute washing period of 100% PDCA, was incorporated to ensure any contaminants built up from the eluents were removed in preparation for the following sample.

3.2 METHOD STABILITY AND REPRODUCIBILITY

To assess the stability of the method with regards to both the chromatographic separation, defined as standard deviation of the retention time, and the peak shape and area reproducibility, seven replicates of a multi-element standard (2.5 ng column load) in 0.5M HNO_3 were measured. Initially 23 elements of interest were investigated and, where possible, multiple m/z traces of the same element were monitored, enabling analysis of the reproducibility and accuracy of isotope ratios. The resulting retention times, together with uncertainty, average peak areas, and 2σ relative standard deviation for all the elements were examined (shown in **Table 6**). The standard deviation in retention times, as shown in brackets in **Table 6**, for all the peaks are < 20 seconds throughout the run; however, europium and praseodymium have a lower tolerance at < 30 seconds. The reproducibility varies slightly, but most signal RSD's are ≤ 10%. The only exceptions are chromium and palladium, and this may be due to the peak-picking software currently not being optimum for these elements.

Table 6. Retention times complete with 2σ standard deviation, average total counts together with 2σ standard deviation (SD), and the relative standard deviation (RSD) of seven replicates of a multi-element standard

Isotope	Retention time with uncertainty (seconds)	Average area (counts)	SD (counts)	RSD
^{142}Ce	1675(18)	4.67E+06	3.12E+05	7%
^{144}Nd	1862(18)	1.18E+07	5.68E+05	5%
^{146}Nd	1862(18)	8.60E+06	4.98E+05	6%
^{147}Sm	1990(16)	6.95E+06	4.24E+05	6%
^{152}Sm	1990(16)	1.45E+07	7.58E+05	5%
^{151}Eu	2070(23)	1.56E+07	1.23E+06	8%
^{153}Eu	2070(23)	1.88E+07	1.65E+06	9%
^{156}Gd	2531(19)	9.75E+06	4.72E+05	5%
^{157}Gd	2531(19)	7.37E+06	3.65E+05	5%
^{158}Gd	2531(19)	1.16E+07	6.15E+05	5%
^{7}Li	129(7)	2.70E+04	1.17E+03	4.3%
^{9}Be	90(3)	6.41E+03	3.76E+02	6%
^{52}Cr	242(4)	5.13E+06	6.42E+05	12%
^{55}Mn	695(5)	4.02E+06	1.37E+05	3%
^{58}Ni	445(3)	4.15E+06	1.76E+05	4%
^{60}Ni	445(3)	1.88E+06	6.63E+04	4%
^{59}Co	553(5)	9.50E+06	4.55E+05	5%
^{63}Cu	383(6)	1.95E+06	1.32E+05	6.7%
^{65}Cu	383(6)	6.73E+05	3.13E+04	4.6%
^{69}Ga	243(2)	2.96E+06	1.87E+05	6%
^{75}As	92(3)	9.64E+05	8.12E+04	8%

^{85}Rb	161(5)	4.05E+06	1.77E+05	4%
^{87}Rb	161(5)	1.88E+06	8.02E+04	4%
^{87}Sr	447(6)	3.63E+05	1.77E+04	5%
^{88}Sr	447(6)	5.06E+06	1.96E+05	4%
^{100}Ru	130(3)	1.02E+06	5.46E+04	5%
^{101}Ru	130(3)	1.37E+06	7.79E+04	6%
^{103}Rh	93(2)	3.35E+07	1.68E+06	5%
^{106}Pd	411(5)	8.98E+05	1.08E+05	12%
^{108}Pd	411(5)	9.33E+05	1.20E+05	13%
^{122}Cd	576(6)	6.64E+06	2.35E+05	4%
^{114}Cd	576(6)	8.00E+06	3.29E+05	4%
^{133}Cs	171(2)	1.60E+07	1.03E+06	6%
^{141}Pr	1795(23)	4.49E+07	2.38E+06	5%
^{205}Tl	240(3)	4.25E+07	2.07E+06	5%
^{193}Ir	92(2)	1.40E+07	8.50E+05	6%

3.3 ISOTOPIC RATIO PRECISION AND ACCURACY

Although peak stability is important to ensure that the developed method is robust enough, isotopic ratio stability is more important when IDMS is to be employed for quantitation. **Table 7** details the average determined peak area ratios, together with the relative standard deviation of seven replicates. The measured ratios of these natural standards are then compared with the actual natural elemental molar ratios.

Table 7. The measured atom % ratios from seven replicates together with the 2σ relative standard deviation (RSD). The natural mole fraction ratio is also given together with the measured ratio/natural ratio

Ratio	Measured Atom% Ratio	2σ -RSD	Natural mole fraction ratio*	Measured ratio/ natural ratio

$^{140}Ce/^{142}Ce$	7.19	1.70%	7.96	90%
$^{144}Nd/^{146}Nd$	1.39	1.00%	1.38	100%
$^{147}Sm/^{152}Sm$	0.48	1.10%	0.56	86%
$^{151}Eu/^{153}Eu$	0.83	1.50%	0.92	91%
$^{156}Gd/^{157}Gd$	1.32	0.40%	1.31	101%
$^{157}Gd/^{158}Gd$	0.63	1.30%	0.63	100%
$^{58}Ni/^{60}Ni$	2.18	1.90%	2.60	84%
$^{63}Cu/^{65}Cu$	2.15	2.00%	2.24	96%
$^{85}Rb/^{87}Rb$	2.15	0.80%	2.59	83%
$^{87}Sr/^{88}Sr$	0.074	3.70%	0.08	87%
$^{100}Ru/^{101}Ru$	0.72	2.00%	0.74	97%
$^{106}Pd/^{108}Pd$	0.96	2.40%	1.03	93%
$^{112}Cd/^{114}Cd$	0.83	1.10%	0.84	99%

*All isotopic data was sourced from the National Nuclear Data Center [65].

The RSD for many of the cases is < 2%, where strontium and palladium are the exceptions, but still show < 4% RSD. The isotope ratio recoveries (measured atom% ratio/calculated atom % ratio) seem to be close to calculated, with the majority being within 15% of calculated. In practice, those with lower accuracy should not pose an issue, as the precision of the measurement is good enough to use a certified natural standard and mass correct. For accurate IDMS concentrations, a mass bias correction involves analyzing a natural multi-element standard alongside the samples at a similar concentration (see also section 3.5). The isotopic ratio recovery from the natural standard is then determined, and the isotopic ratio of the sample is subsequently corrected. The response in the machine appears to be the primary source of the mass bias, however the difference in molar abundance of the isotopes measured, the elution time, and peak shape also appear to influence the bias. The elements with isotopic masses between 58 and 88 appear to show a bias of ~15% for a two mass-unit difference. Copper appears to be the exception with a higher recovery than expected, the reason for this is unclear, and further investigation will be required to understand the recoveries of each of the individual elements. **Table 8** shows the mass bias calculation sheet for the application of a neodymium standard of known at-om/mol% ratios. Here the mass difference between the isotopes and the measured bias show linear correlation. The resulting mass bias curve can, in turn, be plotted and the equation applied to isotopes in the sample that may not present in the mass bias standard

Table 8. Mass bias calculation sheet for the application of a standard of known atom/mol% ratios. The example below is the application of a measured natural neodymium standard to mass bias correct a second neodymium standard of lower concentration. Inset figure: The mass bias correction curve

	Background (counts)	Mass Bias Standard (counts)	Blank corrected (counts)		
Nd-142	5041.72	1845693	1840651		
Nd-143	3284.72	840882	837598		
Nd-144	1400.75	1655457	1654056		
Nd-145	666.79	584368	583701		
Nd-146	3279.2	1228602	1225323		
Nd-148	1253.2	421811	420558		
Nd-150	2154.3	426377	424223		
		Mass Bias corrections			
Natural ratio	Measured	True	Bias	Mass difference from centroid	
142/145	1.113	1.141	97.5%	-2	
143/145	0.506	0.512	99.0%	-1	
144/145	-	-	100.0%	0	
145	0.353	0.348	101.3%	1	
146/145	0.741	0.722	102.6%	2	
148/145	0.254	0.242	105.1%	4	
150/145	0.256	0.237	108.3%	6	

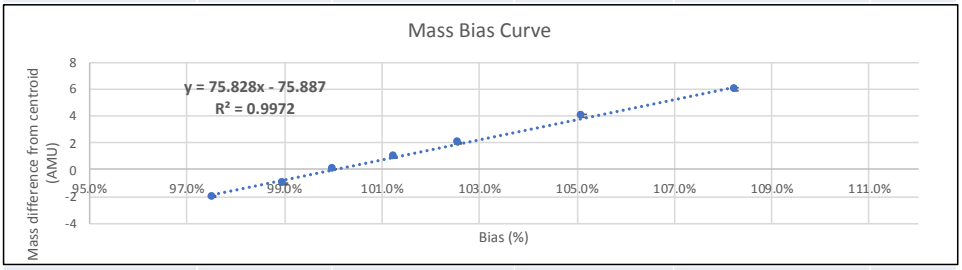

	Background (counts)	Natural SAMPLE (counts)	Blank corrected (counts)		
Nd-142	5041.72	623934	618892		
Nd-143	3284.72	281789	278504		
Nd-144	1400.75	551693	550292		
Nd-145	666.79	197108	196442		
Nd-146	3279.2	409389	406110		
Nd-148	1253.2	142291	141038		
Nd-150	2154.3	145123	142968		
Discrimination Calculations		Calculated Isotopic ratios	**Measured atom%**	**Natural atom% abundance**	**Recovery (%)**
R' 142,144 (Nd142/Nd144)	1.153	Nd-142 atom %	**27.32**	**27.15%**	**101**
R' 143,144 (Nd143/Nd144)	0.511	Nd-143 atom %	**12.11**	**12.17%**	**100**
R' 145,144 (Nd145/Nd144)	0.353	Nd-144 atom %	**23.70**	**23.80%**	**100**
R' 146,144 (Nd146/Nd144)	0.720	Nd-145 atom %	**8.35**	**8.29%**	**101**
R' 148,144 (Nd148/Nd144)	0.244	Nd-146 atom %	**17.05**	**17.19%**	**99**
R' 150,144 (Nd150/Nd144)	0.240	Nd-148 atom %	**5.78**	**5.76%**	**100**
		Nd-150 atom %	**5.69**	**5.64%**	**101**
Sum	3.220	Total atom %	100.0000		
Denominator (1+R' 5,4+R' 6,4+R' 7,4+R' 8,4)	4.220				

3.4 LIMITS OF DETECTION AND QUANTITATION

Table 9 lists the isotopic LOD and LOQ values as determined by linear regression analysis. These values are defined as the amount of material separated on the column for a given injection, based on the current experimental parameters. The values range from low to mid-range picogram levels, with some analytes having LOD values on the femtogram level, which is not achievable on a quadrupole ICPMS using traditional methods. Further weight for the LOQ values is shown when looking at the isotopic ratios of the

standards close in concentration to the LOQ level for each element. For many of the analytes, the measured isotopic ratio at the LOQ was within 3% of that measured at 1.25 ng. The measured ratios at the LOQ were also shown to be within 5-10% of calculated. These values have been determined for an ideal system, with varying matrices and acid concentrations likely having a negative affect for real systems, yielding higher LOD's and LOQ's. These values do, however, give weight to the overall sensitivity of the analytical method.

Table 9. The LOD and LOQ for the individual analytes monitored. The elemental LOD and LOQ refers to the calculated numbers based on a linear regression slope analysis*, and the isotopic LOD and LOQ are calculated by multiplying the elementally determined LOD and LOQ values by the natural isotopic abundance. Also detailed are the determined atom % ratios of the standard closest to the LOQ level, together with the accuracy to the natural mole fraction ratio and the accuracy to the atom % ratio of the 1.25 ng standard (which would be employed as a mass bias standard if IDMS were to be employed).

Isotope	Isotopic LOD (pg)	Isotopic LOQ (pg)	Ratio	Atom % Ratio of Standard Closest in Concentration to LOQ	Natural mole fraction ratio*¥	Accuracy to natural ratio	Accuracy to 1.25 ppb ratio
^{7}Li	48.4	146.5					
^{85}Rb	7	21.1	^{85}Rb /^{87}Rb	2.27	2.59	88%	106%
^{87}Rb	2.8	8.6					
^{133}Cs	8.5	25.7					
^{9}Be	90.4	274					
^{87}Sr	4	12.2	^{87}Sr /^{88}Sr	0.064	0.08	76%	87%
^{88}Sr	37.1	112.4					
^{55}Mn	83.6	253.2					
^{59}Co	14.1	42.6					
^{58}Ni	169.7	514.1	^{58}Ni /^{60}Ni	2.54	2.60	98%	117%
^{60}Ni	76.4	231.6					
^{63}Cu	109.5	331.8	^{63}Cu /^{65}Cu	2.27	2.24	101%	106%

^{65}Cu	43.5	131.8					
^{69}Ga	21.4	64.8					
^{75}As	19.4	58.7					
^{205}Tl	12	36.4					
^{100}Ru	5	15.2	^{100}Ru /^{101}Ru	0.71	0.74	96%	99%
^{101}Ru	5.6	17					
^{103}Rh	16.6	50.2					
^{106}Pd	6.5	19.7	^{106}Pd /^{108}Pd	1.03	1.03	100%	107%
^{108}Pd	2.8	8.5					
^{112}Cd	5.9	17.8	^{112}Cd/^{114}Cd	0.83	0.84	99%	100%
^{114}Cd	7.2	21.9					
^{193}Ir	6.3	19.1					
^{140}Ce	8.1	24.6	^{140}Ce /^{142}Ce	7.48	7.96	94%	104%
^{142}Ce	0.6	1.8					
^{141}Pr	25.9	78.5					
^{142}Nd	0.4	1.2	^{142}Nd /^{144}Nd	1.12	1.14	98%	99%
^{144}Nd	1.8	5.6	^{144}Nd /^{146}Nd	1.38	1.38	100%	99%
^{146}Nd	1.3	3.9	^{142}Nd /^{146}Nd	1.54	1.58	97%	99%
^{147}Sm	2.2	6.6	^{147}Sm /^{152}Sm	0.46	0.56	82%	97%
^{152}Sm	5.2	15.8					
^{151}Eu	1.3	4	^{151}Eu /^{153}Eu	0.86	0.92	94%	104%
^{153}Eu	2	6					
^{156}Gd	2.5	7.7	^{156}Gd /^{157}Gd	1.25	1.31	96%	96%
^{157}Gd	2.3	7.1	^{157}Gd/^{158}Gd	0.61	0.63	97%	96%
^{158}Gd	2.2	6.7	^{156}Gd /^{158}Gd	0.78	0.82	95%	103%

*The standard deviation of the Y-intercept (y) and the slope of the linear regression line (x) were calculated using the Regression Function in the Data Analysis tool in Microsoft Excel. The LOD is defined as 3.3×(y/x) and the LOQ is defined as 10×(y/x).

¥All isotopic data was sourced from the National Nuclear Data Center [65].

3.5 ISOTOPE DILUTION

As further proof of concept that chromatographic peak areas for elementally-separated analytes can successfully be used for isotopic analysis and, thus, IDMS analysis, an IV-ICPMS-71A (10 ug mL^{-1} multi element standard) was spiked with the ORNL-023 enriched-isotope mixed-lanthanide standard. Ideally, for a 1-2% uncertainty analysis, the sample should be spiked within an order of magnitude of the concentration of the analyte to be measured to see a noticeable difference in the isotopic distribution. The method mass bias must also be determined to achieve a 1-2% uncertainty using a quadrupole-based mass spectrometer. In these cases, a natural mixed lanthanide standard was employed as a mass bias standard and a secondary natural mixed lanthanide standard of a concentration close to that of the sample was employed as a control.

Figure 4 shows the chromatograms and resulting peaks for each of the neodymium isotopes in the natural IV-ICPMS-71A standard (left, 125 pg injection) and the natural standard spiked with the ^{150}Nd-enriched IDMS-023 spike (right, 125 pg injection). As can be seen in **Table 10**, for three of the analytes, the accuracy of the analysis was < 1%, with the precision of the measurements being < 2% for both neodymium and samarium. Europium and gadolinium appeared to show poorer precision, likely due to the spike concentration in the ONRL-023 enriched-lanthanide mix used for the analysis being significantly lower than that in the sample. However, it resulted in only a very subtle change in the isotopic distribution of the spiked sample, leading to a larger analytical uncertainty. Additionally, these enriched spikes were specifically chosen to perform IDMS measurements on non-natural lanthanides from previous work performed on spent nuclear fuels and isotope production.

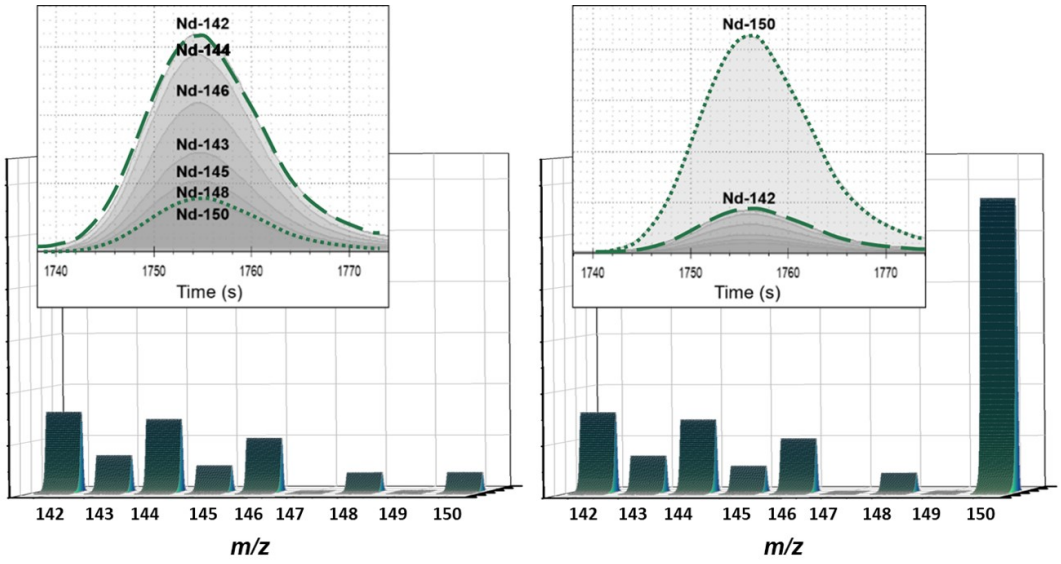

Figure 4. Chromatograms for each of the neodymium isotopes for the natural IV-ICPMS-71A standard (left, 125 pg injection) and the natural standard spiked with the ^{150}Nd enriched IDMS-023 spike (right, 125 pg injection). The ^{142}Nd (long dashes) and ^{150}Nd (short dashes) traces are emphasized in each image for clarity.

Table 10. IDMS recovery numbers for an IV-ICPMS-71A (10ug.mL^{-1n} multi element standard), using IDMS-023 enriched isotope mixed lanthanide standard. Entire IDMS procedure, including data interpretation, was performed in triplicate on two separate days.

Element	Recovery	2σ-std. dev.	Sample:Spike
Nd	99.6%	1.6%	1 : 1.11
Sm	99.9%	1.8%	1 : 0.35
Eu	99.7%	15.6%	1 : 0.03
Gd	102.6%	6.6%	1 : 0.04

3.6 ANALYSIS IN SURROGATE SOIL MATRIX

The next stage in the method development was to apply the optimized separation scheme to analytes within a synthetic soil matrix. For the RAPID method to be effective with analyzing complex nuclear materials, it must be robust enough to overcome the highly complex matrices of potential samples. Complex matrices can have a serious impact on the sensitivity, reproducibility, and stability of a measurement, with high salt

content potentially resulting in the failure or clogging of the nebulizer, as well as the potential to damage the instrument cones, lenses, ion optics, and the detector. The matrix type to be investigated was a trace-clean synthetic soil matrix based on the relative elemental composition of the NIST 2711a standard Montana II soil. The soil surrogate was required to provide a realistic matrix while maintaining the ability to determine the method detection limits using linear regression as detailed in Section 2.4. Primarily composed of oxygen, nitrogen, silicon, magnesium, aluminum, iron, and calcium (see **Table 11**), the soil surrogate was doped with varying levels of 48 elements post-digestion.

Preparation of the surrogate soil was carried out with the use of the compounds detailed in **Table 11**, chosen for their availability in trace-metals grade. The nature of the trace-metals grade compounds, in particular the aluminum nitrate, meant the elemental mass fractions were ~50% from those reported on the NIST SRM-2711a certificate (also listed in **Table 11**). Although complete digestion was not the primary concern of this study, both trace elements and elemental mass fractions were verified by quadruple ICPMS prior to elemental spiking. Recoveries of the primary elements in the soil surrogate were verified via triplicate digestions of 200 mg of the soil surrogate into ca. 15 mL were > 80% in all cases, the silicon being the most difficult element to quantify via ICPMS.

Table 11. Elemental composition of surrogate NIST 2711a soil, showing the elemental source and weight fractions.

Element	Compound mass fractions (%)	Elemental mass fractions (%)*	Elemental mass fractions in NIST 2711a (%)
Si (Silicon dioxide, SiO_2)	38.0	17.7	31.4
Al (Aluminum nitrate nonahydrate, $Al(NO_3)_3 \cdot 9H_2O$)	51.4	3.7	6.72
Fe (Iron(III) oxide, Fe_2O_3)	2.2	1.6	2.82
Ca (Calcium oxide, CaO)	1.9	1.3	2.42

Mg (Magnesium nitrate hexahydrate, $Mg(NO_3)_2 \cdot 6H_2O$)	6.6	0.6	1.07

*remaining elemental weight fraction (*ca.* 75%) is comprised of oxygen, nitrogen, and hydrogen

Post digestion, the surrogate soil, determined to have ~2.5 mg/mL silicon, was spiked with an elemental standard mix composed of the elements listed in **Table 11** (for the element sources, see **Table 2**) yielding a ~500 ng/mL elemental sample. To determine the effect of the surrogate soil matrix on the stability of the method and performance of the ICPMS over an extended period, nine replicates of a 50 µL injection a of a 100 ng/mL multi-element sample in the surrogate soil matrix was investigated (5× dilution in HNO3, 2%, ~0.5N). Each sample injection was bracketed by two blank analyses to both clean the column between replicates and to extend the run to a ca. 24 h period. **Table 12** illustrates the method reproducibility by giving 2σ relative standard deviations of the measured peak areas for each element (RSD) for the 48 elements together with their elution times in the surrogate matrix and, where measured, the original elution time as detailed in **Table 6**.

Table 12. Elemental retention times in the original method development study and the surrogate soil matrix, together with the measured RSD of the nine replicates over the 24 h period

Element	Tracer	Retention time (s)		Shift due to matrix (s)	Stability over 24 h period¥ (if measured) RSD 9 replicates (%)	Natural and non-natural isobaric interferences
		In dissolved surrogate soil matrix	In 5% HNO_3			
Barium	^{138}Ba**	90			60.0	Ce, La, Nd
Arsenic	^{75}As**	92			6.8	
Iridium	^{193}Ir**	92	92	0	40.0	Re, Pt, Os
Selenium	^{77}Se**	92			59.0	
Ruthenium	^{101}Ru	100/350	130/400	−50	6.6	Rh, Pd, Cd, Ag
Tellurium	^{125}Te	100			5.2	

Scandium	^{45}Sc	110			11	Ca*, Ti, V
Neptunium	^{237}Np	120			2.2	U*
Niobium	^{93}Nb	123			6.2	
Lithium	^{7}Li	126	129	−3	3.4	Be
Osmium	^{189}Os	126			8.7	
Rubidium	^{87}Rb	157	161	−4	3.5	
Cesium	^{133}Cs	165	190	−25	3.6	
Thallium	^{205}Tl	250	240	10	1.4	Ba, La, Ce
Tin	^{118}Sn	250			7.0	
Titanium	^{49}Ti	251			N/A	
Gallium	^{71}Ga	253			4.6	Zn, Co
Rhodium	^{103}Rh	270			21.0	Ru, Pd
Iron	^{58}Fe	276			N/A	Cr, Mn, Co, Ni
Lead	^{208}Pb	278			2.1	Hg, Tl*, Bi, Po*
Zinc	^{66}Zn	296			N/A	Cu
Copper	^{65}Cu	398	383	15	N/A	Zn, Ga
Palladium	^{105}Pd	427	411	16	N/A	
Strontium	^{87}Sr	750	747	3	3.5	Y, Zr
Nickel	^{60}Ni	460	445	15	N/A	Fe, Cu, Zn
Cobalt	^{59}Co	575	553	22	40.0	Ni, Fe
Cadmium	^{112}Cd	595			2.3	In
Gold	^{197}Au	606			7.9	Pt, Os, Ir, Hg
Tantalum	^{181}Ta	607			5.3	Hf, Re, W
Manganese	^{55}Mn	720	695	25	40.0	Fe
Antimony	^{121}Sb	1020			6.2	
Lanthanum	^{139}La	1473			3.0	
Cerium	^{142}Ce	1600	1675	−75	3.0	Pr, Nd, Sm, Pm
Praseodymium	^{141}Pr	1692	1795	−103	3.2	Nd, Ce, Pm
Germanium	^{73}Ge	1750			5.7	

Neodymium	^{146}Nd	1760	1862	−102	2.5	Sm, Gd, Eu, Pm
Samarium	^{147}Sm	1830	1990	−160	2.0	
Europium	^{153}Eu	1865	2070	−205	1.8	Sm, Gd*, Dy
Gadolinium	^{157}Gd	1882	2131	−249	3.4	
Terbium	^{159}Tb	1945			3.0	
Curium	^{244}Cm	1950			1.8	Am*
Americium	^{241}Am	1970			1.7	Cm*, Pu
Dysprosium	^{163}Dy	1990			1.7	
Yttrium	^{89}Y	2013			5.0	
Holmium	^{165}Ho	2,040			2.4	
Plutonium	^{239}Pu	2250			10.0	Am, Cm
Thorium	^{232}Th	2310			3.8	Ra, U
Thulium	^{169}Tm	2910			3.0	
Zirconium	^{94}Zr	2,280			4.9	

Note: The natural and non-natural isobaric interferences are also listed.

N/A = not applicable; RSD = relative standard deviation.

*Indicates that the element will have potential isobaric overlap or that the element has not or cannot be monitored.

**The nature of the peaks at t=90-100s is difficult to discern, the apparent stability likely reflects either contamination in the eluents or remnants from previous injections that build up on the resin and are paritially eluted in the nitric acid matrix of the following injection. The issues of column contaminant loading and sample cross-contamination for certain elements will be considered in future work.

¥ a total of 27 samples were injected as each standard was bracketed with blank injections.

When compared to the primary study carried out in a simple 5% HNO3 matrix, the elution times for the majority of the analytes that elute in the first 720 seconds (during the isocratic PDCA elution) do not vary by more than 30 seconds. The major shifts in retention times appear to be occurring during the gradient DGA/oxalic acid elution section, in which the lanthanides are eluted. The high concentration of fluoride ions in solution is a potential cause of these retention shifts, although excess fluoride should be bound as BF3 due to the excess boric acid employed in the third digestion stage. Another possible cause for a shift in lanthanide elution is a potential change in pH of the oxalic acid eluent. Although eluent buffering using

ammonium hydroxide makes the eluent more compatible with direct analysis via ICPMS due to salt-less combustion of the eluent, a downside is that the pH of the eluent can change over time. One thing of note is the split elution of the ruthenium isotopes at ~100 s and ~350 s, the two retention times could possibly correspond with ruthenium existing in two different oxidation states in solution, although the nature of the ruthenium species is not known, and further study would be required to confirm this observation.

An initial investigation determined that the neat digest resulted in both peak broadening and splitting, likely due to the high fluoride content. A 50 µL injection of a 5× dilution in HNO3 (2%, 0.5M), a ca. 10 µg silicon and ~2.5 ng analytes column load, resulted in the chromatogram in **Figure 5** superimposed onto the elution profile.

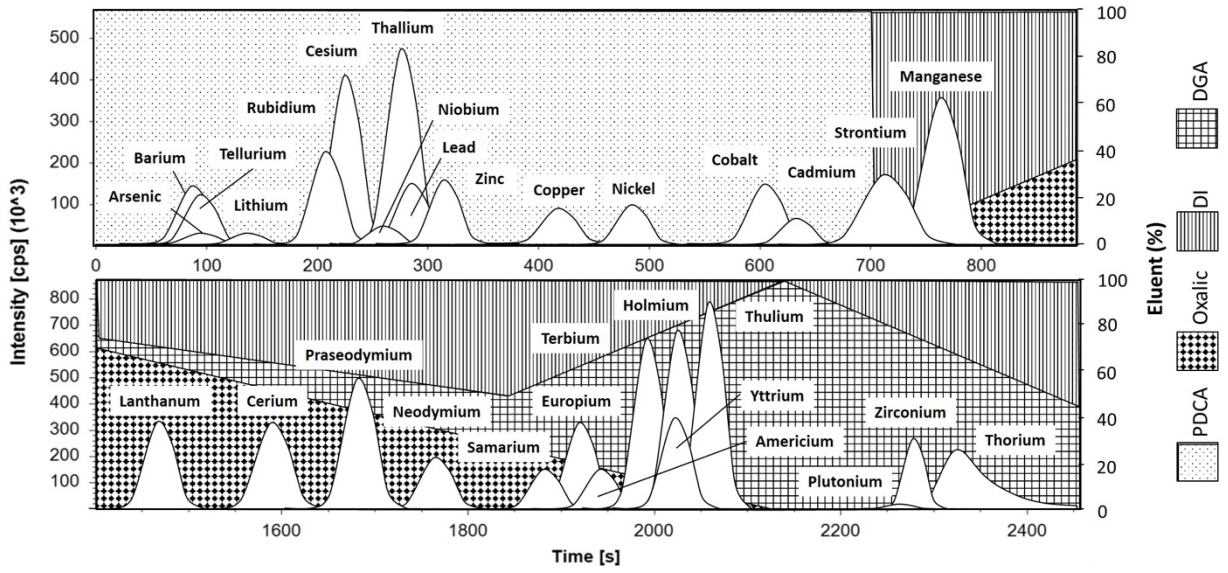

Figure 5. Chromatogram, with the gradient elution profile overlaid, illustrating 30 of the 48 elements monitored in the surrogate soil matrix with the t = 0 - 900 s region of the chromatogram illustrated above, showing each of the individual analytes in more detail, including isotopic sensitivity, peak shape, retention time, isobaric and elemental overlap, and peak tailing. Below shows a partial chromatogram of t = 1400 – 2400 s.

Despite inclusion of the surrogate soil matrix, the elements of interest have clean peak resolution, good peak shape with minimal peak tailing, and, despite visible elemental overlap, complete isobaric separation of all natural and non-natural isotopes. The analysis of a 100× dilution of the surrogate soil digests

determined that the majority of the elemental mass (Si, Al, and Ca) elute at or near the solvent front (ca. 90-110 s, see **Figure 6**) and appear to have little impact on the measurement of other elements. Monitoring the m/z 57 and m/z 24, iron and magnesium are shown to elute at 236 s and 98 9s respectively. Due to the organic components of the eluents, incomplete combustion in the plasma likely leads to the formation of polyatomic species resulting in interferences in the m/z 29 and m/z 44 chromatograms. The polyatomic species observed are likely to be [COH]+ on m/z 29 and [CO2]+ on m/z 44.

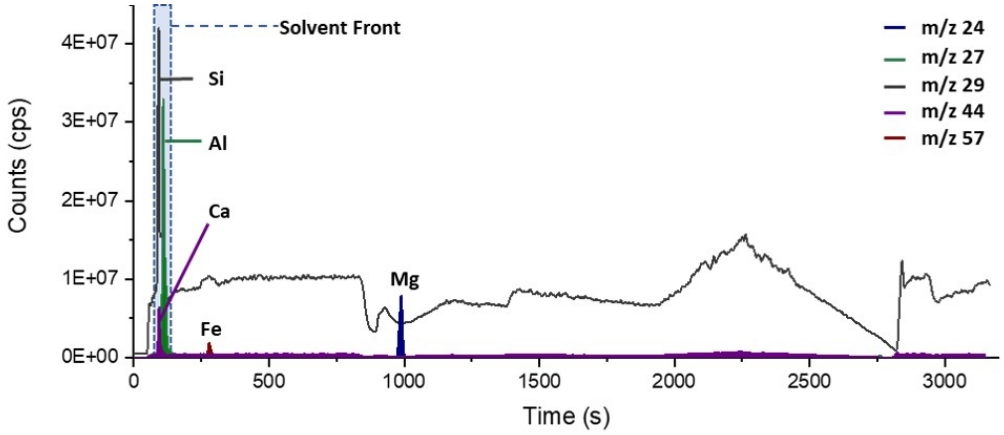

Figure 6. Shows the overlaid chromatograms of a 100× dilution of the surrogate soil digest. The m/z 24, 27, 29, 44, and 57 were monitored and the individual elements eluting as follow Si and Ca at 90 s, Al at 100 s, Fe at 239 s, and Mg at 989 s.

The designation of these interferences as organic polyatomic is strongly based on the changing levels of these signals being in line with the changing levels of the eluents as can be seen in **Figure 7**, where the m/z 29 and m/z 44 chromatograms have both been normalized to the elution profile for clarity. If necessary, some of the polyatomic species could be reduced by the introduction of an oxygen bleed into the plasma, or by use of the collision cell and the kinetic energy discriminator mode available.

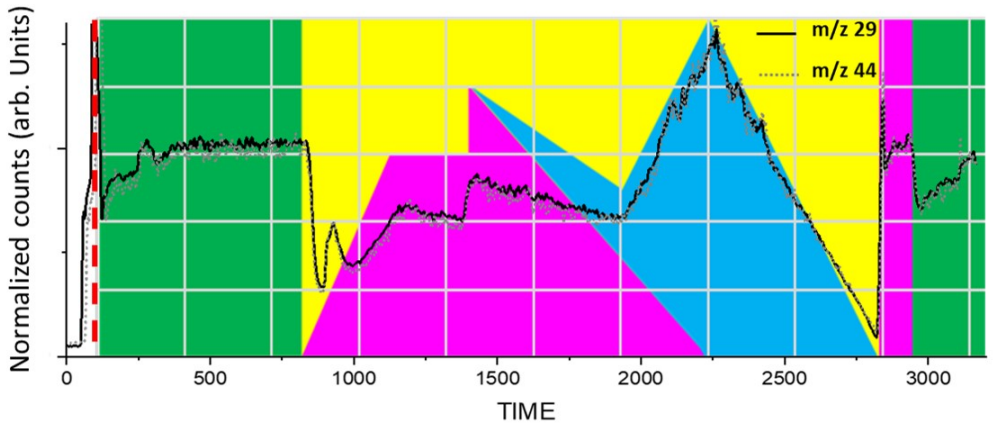

Figure 7. The normalized m/z 29 and m/z 44 chromatograms showing distinct changes in signal in line with the changes in the gradient elution profile (overlaid, deionized water (yellow), 6 mM PDCA (green), 100 mM oxalic acid (pink), and 100 mM DGA (blue)). Note: a ca. 90s delay between the elution profile timing and the ICPMS signals, the time required for the eluent to travel from the gradient mixing pump to the detector of the ICPMS (also defined as the solvent front).

The 100 ng/mL multi-element sample in the surrogate soil matrix was diluted using the surrogate soil matrix, resulting in a series of low-level standards with elemental column loading ranging from 5 to 500 pg. Using linear regression analysis, as described in Section 2.5, the determined isotopic LODs and LOQs are tabulated in **Table 13** together with those determined in the 5% HNO_3 matrix study.

Table 13. LODs and LOQs for the individual isotopes monitored both with and without a dissolved surrogate soil matrix

Isotope	Isotopic LOD (no matrix) (pg)	Isotopic LOD (surrogate soil matrix) (pg)	Isotopic LOQ (no matrix) (pg)	Isotopic LOQ (surrogate soil matrix) (pg)	Comments
^{7}Li	48.4		146.5		Matrix Background
^{85}Rb	7.0	1.6	21.1	4.7	
^{87}Rb	2.8		8.6		Not Analyzed
^{133}Cs	8.5	1.6	25.7	4.8	
^{9}Be	90.4	2.4	274.0	7.4	
^{87}Sr	4.0		12.2		Not Analyzed

^{88}Sr	37.1		112.4		Matrix Background
^{55}Mn	83.6		253.2		Matrix Background
^{59}Co	14.1		42.6		Matrix Background
^{58}Ni	169.7		514.1		Matrix Background
^{60}Ni	76.4		231.6		Matrix Background
^{63}Cu	109.5		331.8		Matrix Background
^{65}Cu	43.5		131.8		Matrix Background
^{69}Ga	21.4		64.8		Not Analyzed
^{75}As	19.4		58.7		Not Analyzed
^{205}Tl	12.0	0.7	36.4	2.2	
^{100}Ru	5.0		15.2		Not Analyzed
^{101}Ru	5.6	*6.6*	17.0	*20.1*	
^{103}Rh	16.6	1.3	50.2	3.9	
^{106}Pd	6.5		19.7		Not Analyzed
^{108}Pd	2.8		8.5		Not Analyzed
^{112}Cd	5.9	1.9	17.8	5.9	
^{114}Cd	7.2	1.0	21.9	2.9	
^{193}Ir	6.3	1.1	19.1	3.3	
^{140}Ce	8.1	*7.6*	24.6	*22.9*	High Background
^{142}Ce	0.6	*8.1*	1.8	*24.7*	High Background
^{141}Pr	25.9	0.5	78.5	1.5	
^{142}Nd	0.4	0.7	1.2	2.1	
^{144}Nd	1.8	0.7	5.6	2.0	
^{146}Nd	1.3	1.3	3.9	3.9	
^{147}Sm	2.2	1.5	6.6	4.5	
^{152}Sm	5.2	1.1	15.8	3.3	
^{151}Eu	1.3	0.8	4.0	2.3	
^{153}Eu	2.0	1.0	6.0	3.0	
^{156}Gd	2.5	0.8	7.7	2.5	
^{157}Gd	2.3	1.3	7.1	4.0	
^{158}Gd	2.2	0.9	6.7	2.8	

Notes: Italics denote an incomplete data set due to high analyte matrix in the background. The elemental LODs and LOQs were calculated based on a linear regression slope analysis, and the isotopic LODs and LOQs were calculated by multiplying the elemental numbers by the natural isotopic abundance. *The standard deviation of the y-intercept (y) and the slope of the linear regression line (x) were calculated using the regression function in the Analysis Toolpak in Microsoft Excel. The LOD is defined as 3.3×(y/x), and the LOQ is defined as 10×(y/x).

For most of the isotopes monitored in the surrogate soil matrix, the LOD and LOQ values were the same as or lower than those determined during method development. The likely reason for lower values is a more accurate regression analysis, due to lower concentration standards being used in this study when compared to the original investigation (the highest con-centration standard being 500 pg vs 2500 pg in the original study). Several isotopes previously monitored were excluded from this experiment, as they were found to be present in the surrogate soil matrix at levels two to three orders of magnitude above the LODs previously determined for those analytes. For certain isotopes (^{142}Ce in this case), elevated detection limits were measured relative to the previous study, due to the presence of that isotope in the matrix in trace amounts. In these cases, the LOD and LOQ values could be calculated in the traditional manner of 3.3× and 10× the standard deviation of triplicate analysis of seven replicates of the matrix blank, acquired over three non-consecutive days. This is unimportant for this study, as a conservative LOD or LOQ value for ^{142}Ce can be applied based on the ^{140}Ce value.

3.7 ANALYSIS OF LANTHANIDE CONCENTRATIONS IN A NIST CERTIFIED SOIL, SRM2711A

The final stage in the method development was to combine the optimized separation scheme, IDMS, and a complex soil matrix. NIST SRM 2711a standard Montana II soil was the ideal candidate to test the RAPID protocol combined with IDMS as the concentration of a number of the lanthanide elements are known as either certified, reference, or information values with associated uncertainties [66]. The soil drying, and isotope dilution of the soil followed protocols detailed by NIST in the special report “Certification of Three NIST Renewal Soil Standard Reference Materials for Element Content: SRM 2709a San Joaquin Soil, SRM 2710a Montana Soil I, and SRM 2711a Montana Soil II” [67]. The digestion acids and protocol follow an in-house certified method for the digestion of silica-based materials, chosen for its ability to completely digest the soil sample in under 2 h, while stabilizing over 40 trace elements in the resultant digest. ORNL-

024 is an in-house certified mixture of enriched lanthanides combined by weight specifically for this IDMS analysis. Duplicate portions of SRM 2711a were spiked by weight with ORNL-024 and digested as detailed in section, process blanks and unspiked SRM 2711a samples were also analyzed. **Figure 8** shows a plot of the m/z traces for the mass range 136-160 chromatograms for one replicate of the SRM2711a soil digest spiked with ORNL-024.

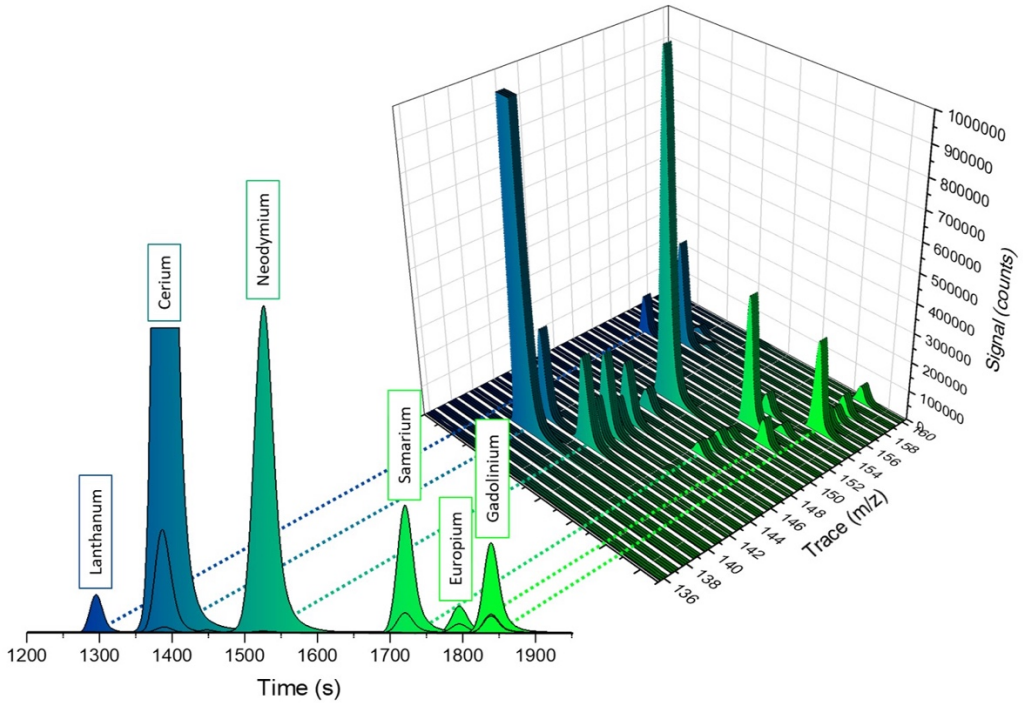

Figure 8. A staggered plot of the m/z 136-160 chromatograms for one replicate of the SRM2711a soil digest spiked with the enriched isotope mix for IDMS measurements with the enriched isotopes ^{140}Ce, ^{150}Nd, ^{152}Sm, ^{151}Eu, and ^{155}Gd clearly visible. Inset: partial chromatograms indicating the elution time of the individual elements.

Clear elemental separation is visible, as are the enhanced signals for the enriched isotopes ^{140}Ce, ^{150}Nd, ^{152}Sm, ^{151}Eu, and ^{155}Gd. The ^{139}La and ^{141}Pr signals have been removed for figure clarity, however the ^{139}La^{16}O and ^{141}Pr^{16}O signals, potential interferences on ^{155}Gd and ^{157}Gd, can be seen at 1300 and 1460s respectively on the m/z 155 and 157 traces. ^{140}Ce^{16}O and ^{142}Ce^{16}O, potential interferences on the ^{156}Gd and ^{158}Gd signals can also be observed at 1400 s. Without the online separation a bias on the gadolinium concentration would definitely have been observed using traditional mass spectrometry techniques. For this

study the concentration of the oxalic acid eluent was raised to 150 mM and resulted in a quicker elution time for the lanthanide elements without compromising peak resolution.

Table 14 shows the 2σ standard deviation of 6 replicate analyses yielded a 1-3% precision, comparable to that observed for the IDMS samples analyzed without a matrix, see Section 3.5. The 2σ standard deviation of 6 replicates of 2 independently dried, spiked, and digested SRM2711a samples also yielded a 1-3% uncertainty for the majority of the analytes, with only cerium showing a lower precision, potentially due to issues with digestion. Samarium was the only NIST certified value on the certificate with the RAPID method yielding higher precision and a value well within the uncertainty of the NIST analyses. The determined neodymium and europium also show higher precision than the reference values provided on the certificate and are well within the uncertainty provided. The concentrations provided for cerium and gadolinium were information values only, however the NIST report for the certification of SRM2711a provides more details of the analyses performed and confirms that there were issues in obtaining cerium values that corresponded to one another.

Table 14. IDMS determined concentrations of cerium, neodymium, samarium, europium, and gadolinium in NIST SRM2711a Montana II soil. The error represents 2σ standard deviation of 6 replicates of 2 independently dried, spiked, and digested SRM 2711a samples.

	Cerium (µg/g)	Neodymium (µg/g)	Samarium (µg/g)	Europium (µg/g)	Gadolinium (µg/g)
RAPID A (2σ STD)	70(3)	32.5(4)	6.1(1)	1.10(5)	5.0(1)
RAPID B (2σ STD)	75(2)	33.5(4)	6.2(1)	1.14(2)	5.1(1)
Average (2σ STD)	72(5)	33(1)	6.15(10)	1.12(4)	5.05(6)
SRM 2711a Certificate Value	70*	29(2)#	5.93(28)¥	1.1(2)#	5*
INAA (2σ STD)	77(4)	32(4)	6.1(5)	1.10(2)	5.1(1)
PGAA (2σ STD)	-	-	5.82(8)	-	-
ICPMS (2σ STD)	66(2)	-	-	-	-
ICP-AES (2σ STD)	66(2)	30(2)	-	-	-
ED-XRF (2σ STD)	62(6)	26(10)	-	-	-

¥Certified Value, #Reference Value, *Information Value

4. RESULTS AND DISCUSSION – SECTION II

The HPIC elution scheme employed in this study is as described in section 3.1. A two-minute washing period of 100% oxalic acid, followed by a five-minute washing period of 100% PDCA was incorporated to ensure any contaminants built up from the eluents were removed in preparation for the following sample. The resulting separation scheme, together with the approximate elution times of the elements of interest, is graphically represented in **Figure 9**.

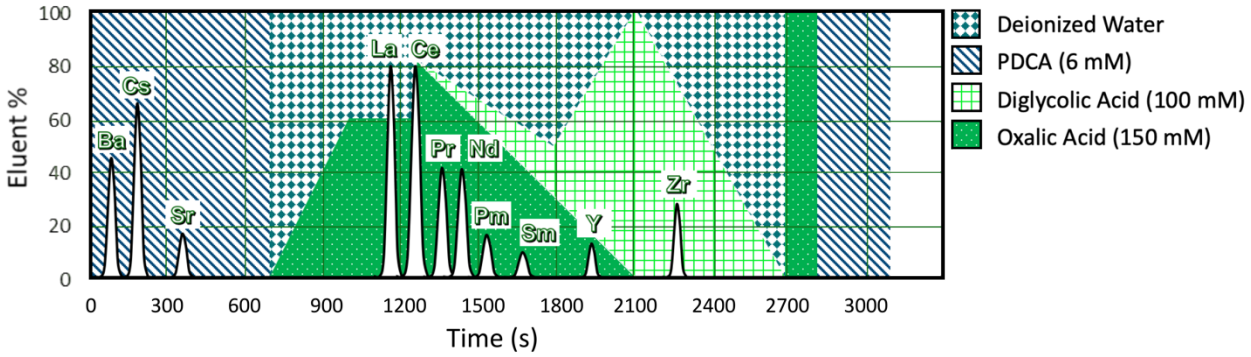

Figure 9. The gradient elution profile, with the corresponding elution times illustrated, for the elemental isolation of the fission elements of interest (cesium, strontium, lanthanum, cerium, praseodymium, neodymium, promethium, samarium, and yttrium). Barium and zirconium are also pictured as these are two of the key elements that have isobaric interferences for cesium, yttrium, and strontium.

The irradiated ^{235}U target leachate was analyzed for fission product isotopic content 178 h post-irradiation, focusing on the lanthanide elements (**Figure 10**), as well as cesium (**Figure 11**), strontium, and yttrium (**Figure 12**). A 50 µL sample of a 2× dilution of the leachate, the equivalent of 20 fg–10 pg of each isotope, was injected with the HPIC system and eluted directly into the iCAP Q ICPMS at 1 mL/min using the elution protocol shown above. The transient *m/z* signals, directly monitored by ICPMS, show elemental separation by peak elution time, resolving isobaric and polyatomic mass interferences. The resulting peaks with the same elution time, after smoothing and peak fitting, are integrated, and their areas are directly related to their atomic percent abundance in the sample. For the majority of the analytes natural contamination was not observed in the sample to any measurable degree, the strontium and yttrium isotopes

were the exception. The m/z traces for these analytes required background subtraction of a matrix blank, resulting in much noisier baselines than observed for the other analytes. This was confirmed to be due to the presence of trace levels of natural strontium and zirconium in the eluents (10-50 pg/mL), which had an impact on the m/z traces 88 and 90.

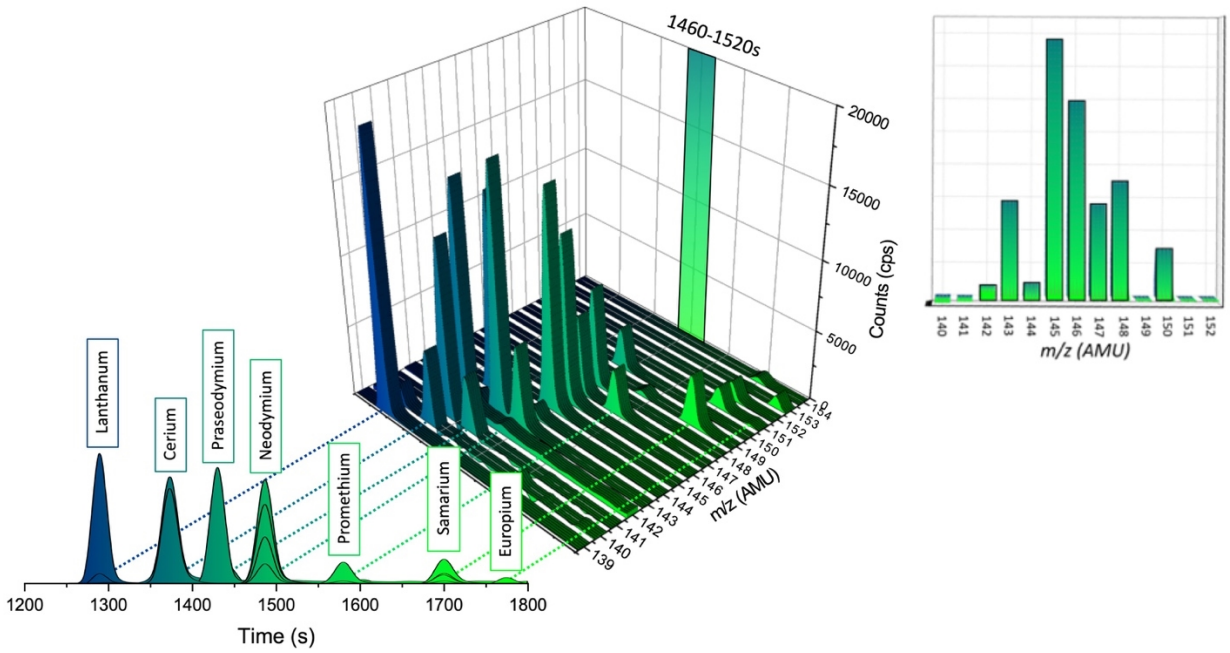

Figure 10. The transient ICPMS signals for m/z 139–154, encompassing the lanthanide elements, from 1200–1800 s elution time (left) for a 50 µL injection of the irradiated target leachate 178 h post-irradiation. The central figure depicts the same transient signals separated by m/z, clarifying which isotopes have isobaric interferences. By limiting the elution time to encompass a single element, in this case, neodymium at 1460–1520 s, then rotating the figure to remove the "Time" axis, the atomic percent abundances of the neodymium isotopes can be observed (right).

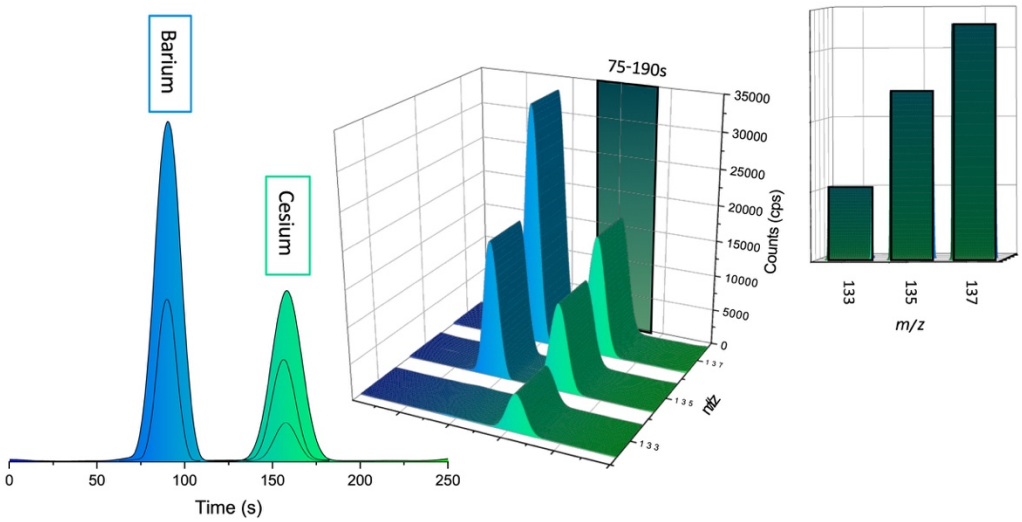

Figure 11.The transient ICPMS signals for m/z 133, 135, and 137, the neutron-induced fission masses for cesium, for a 50 µL injection of the irradiated target leachate 178 h post-irradiation (left). The central figure depicts the same transient signals separated by m/z, showing a clear separation between cesium isotopes and those of both natural and fission-induced barium isobars ^{135}Ba and ^{137}Ba. By limiting the elution time to encompass a single element, in this case, cesium at 75–190 s, then rotating the figure to remove the "Time" axis, the atomic percent abundances of the neutron-induced fission isotopes of cesium can be observed (right).

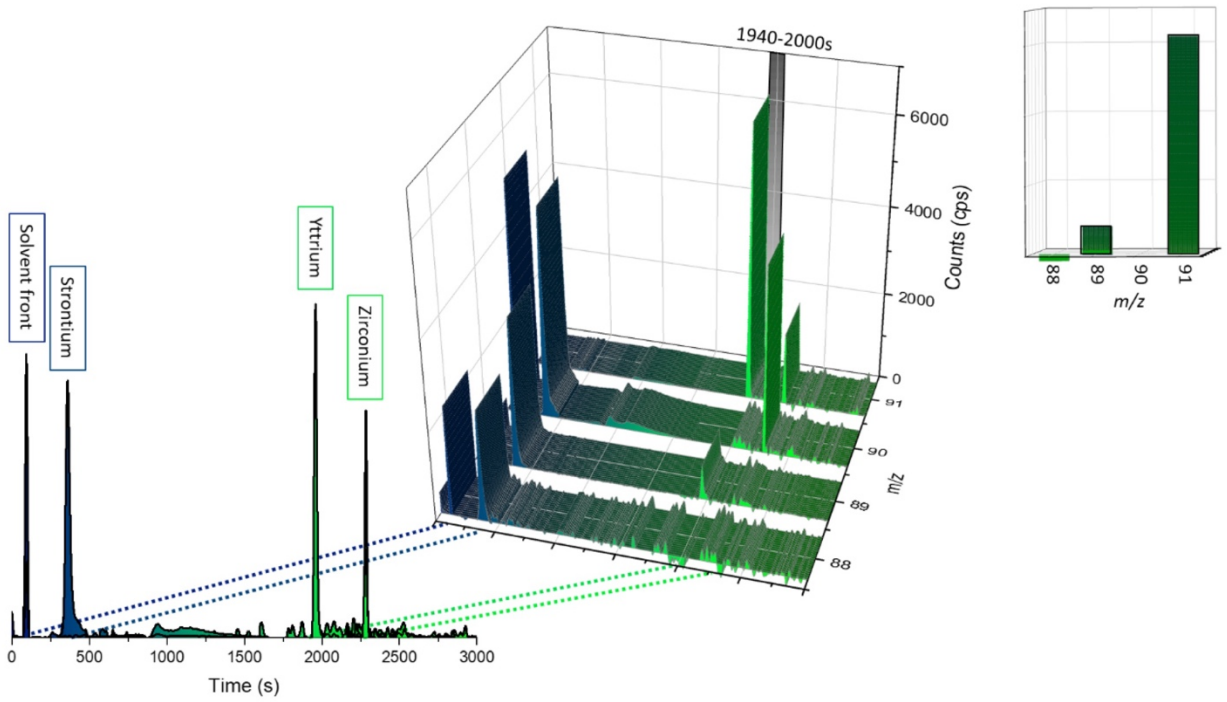

Figure 12. The transient ICPMS signals for m/z 88–91, the neutron-induced fission masses for strontium and yttrium, for a 50 µL injection of the irradiated target leachate 178 h post-irradiation (left). The central figure depicts the same transient signals separated by m/z, showing a clear separation between the isobars ^{89}Sr/^{89}Y, ^{90}Sr/^{90}Zr, and ^{91}Y/^{91}Zr. Separation from the solvent front, and from natural zirconium contamination, is important for accurate isotopic analyses. By limiting the elution time to encompass a single element, in this case, yttrium at 1940–2000 s, then rotating the figure to remove the "Time" axis, the atomic percent abundances of the neutron-induced fission isotopes of yttrium can be observed.

4.1 MASS BIAS CORRECTION

Two independent lots of a mixed-element standard of natural isotopic abundance were analyzed before and after each sample to determine and quantify the mass bias of the iCAP Q quadrupole mass analyzer for each element. The measured isotopic ratios for each element were compared with known values [68], and a quadrupolar bias towards the heavier isotopes was observed. For each analysis, the measured biases were plotted as a function of the percent deviation from a centroid isotope per AMU. A linear fit over the entire mass range for each element yielded equations that could be applied to elements of both natural and non-natural isotopic abundance. The primary mixed-element standard was used to determine the mass bias, and

the secondary standard was used as a control to ensure the bias applied to the analyzed samples was accurate. For the lanthanide elements, it was determined that there was ~1.5% bias per AMU from a centroid isotope. An example of this correction can be found in the supplementary information (**Table 8**). For non-naturally occurring isotopes, ^{147}Nd for example, a linear plot for the naturally-occurring isotopes was calculated and the bias for ^{147}Nd could then be interpolated. For elements with only a single naturally-occurring isotope (i.e. La, Pr, and Y), the calculated mass bias for a neighboring element was applied. For promethium, an element with no naturally-occurring isotopes, the mass bias calculated for the mass difference of the naturally-occurring ^{147}Sm and ^{149}Sm isotopes was employed.

4.2 PRECISION AND BIAS OF ISOTOPIC ANALYSIS

The irradiated leachate was analyzed on three occasions over the course of six weeks. For each analysis, three replicates were analyzed over a 2.5 h period and, post mass bias correction, the average atomic percent abundances for each element were calculated. The precision of the measurement, shown in **Table 15** as a 2σ standard deviation of the replicates, was heavily dependent on the quantity of each element analyzed, the number of neutron-induced fission isotopes monitored for each element, and the atomic percent abundance of each isotope. The levels of isotopes analyzed ranged from ~20 fg (e.g. ^{135}Sm) to ~10 pg (e.g. ^{145}Nd) with the majority of the highly-abundant isotopes showing a 1–3% precision and a 1–2% accuracy when compared with the ORIGEN predictions at each time post-irradiation.

Table 15. The measured average atomic percent (at. %) abundances together with the ORIGEN-predicted atomic percentage for each isotope at t = 178 h, 504 h, and 1018 h post-irradiation. The precision of the measurement is a 2σ standard deviation of the replicates

Time Post Irradiation (h)	**178**		**504**		**1018**	
Isotope	RAPID (meas. at. %) (2σ, n=3)	ORIGEN (calc. at. %)	RAPID (meas. at. %) (2σ, n=3)	ORIGEN (calc. at. %)	RAPID (meas. at. %) (2σ, n=3)	ORIGEN (calc. at. %)
^{88}Sr	**26.5(3)**	26.2	**27.5(10)**	27.7	**29.3(9)**	29.8

^{89}Sr	**31.1(2)**	31.4	**27.7(7)**	27.5	**21.5(3)**	22.1
^{90}Sr	**42(2)**	42.4	**45(1)**	44.8	**49.1(6)**	48.1
^{89}Y	**7.7(8)**	7.9	**20.5(7)**	21.0	**37.3(6)**	37.1
^{91}Y	**92.3(8)**	92.1	**79.5(7)**	79.0	**62.7(6)**	62.9
^{133}Cs	**14.8(2)**	22.7	**14.5(3)**	33.4	**15.2(6)**	35.0
^{135}Cs	**35.5(6)**	38.7	**34.6(14)**	33.4	**35(1)**	32.6
^{137}Cs	**49.7(8)**	38.6	**50.9(15)**	33.2	**49.7(8)**	32.4
^{139}La	**91.5(3)**	91.6	**95.68(5)**	95.6	**98.5(3)**	98.6
^{140}La	**8.4(3)**	8.4	**4.32(5)**	4.4	**1.5(3)**	1.4
^{140}Ce	**8.4(2)**	8.2	**20.1(17)**	21.2	**31.2(4)**	29.4
^{141}Ce	**26.2(5)**	27.6	**20.8(7)**	19.8	**12.6(4)**	12.7
^{142}Ce	**34(2)**	32.2	**31.6(4)**	31.1	**30.2(4)**	31.3
^{143}Ce	**0.76(4)**	0.8	**0.07(3)**	0.0	**0(0)**	0.0
^{144}Ce	**30.3(4)**	29.8	**27(1)**	27.8	**26.0(6)**	26.6
^{141}Pr	**15.4(4)**	15.9	**48(1)**	48.9	**82.3(6)**	82.0
^{143}Pr	**84.6(4)**	84.1	**52(1)**	51.1	**17.7(6)**	18.0
^{143}Nd	**10.9(3)**	11.8	**26.3(5)**	27.0	**33.7(4)**	34.4
^{144}Nd	**0.92(14)**	0.8	**2.5(2)**	2.0	**3.5(2)**	3.6
^{145}Nd	**32.6(4)**	32.2	**28.4(13)**	28.4	**26.4(5)**	25.9
^{146}Nd	**25(1)**	24.6	**21.5(3)**	21.6	**19.8(3)**	19.8
^{147}Nd	**11.3(2)**	11.5	**4.15(11)**	4.2	**1.0(1)**	1.0
^{148}Nd	**13.6(5)**	13.7	**12.4(9)**	12.1	**11.3(2)**	11.0
^{150}Nd	**5.6(4)**	5.4	**4.8(6)**	4.7	**43(2)**	4.3
^{147}Pm	**88.7(5)**	88.5	**99.9(1)**	99.9	**100.0(1)**	100.0
^{149}Pm	**11.3(5)**	11.5	**0.08(1)**	0.1	**0(0)**	0.0
^{147}Sm	**0(0)**	0.0	**0.8(4)**	0.8	**2.7(1)**	2.4
^{149}Sm	**54.6(6)**	56.0	**57(2)**	58.2	**56(2)**	57.3
^{151}Sm	**23(1)**	23.8	**22(2)**	22.6	**22.2(5)**	22.2
^{152}Sm	**17(1)**	15.3	**15(1)**	14.4	**14(1)**	14.1
^{153}Sm	**0.62(7)**	0.6	**0.01(3)**	0.0	**0(0)**	0.0
^{154}Sm	**4.5(6)**	4.3	**5(1)**	4.0	**4.9(4)**	3.9

It can be seen in **Table 15** that the measured cesium isotopic compositions do not agree with the ORIGEN-predicted values. Initially, barium interferences were thought to be influencing the cesium

isotopic measurements; however, as can be seen in **Figure 11**, clear separation of barium and cesium is observed. The unexpected cesium isotopic composition is likely due to the parent fission isotopes for the cesium isotopes being xenon. The low abundance of ^{133}Cs relative to the ^{135}Cs and ^{137}Cs indicates a potential breach in the ampoule prior to crushing and leaching for this analysis. Using the ORIGEN model, it was determined that the composition of the cesium was fixed at ~24 h post-irradiation, corresponding with the removal of the pellet from the decay station (**Table 16**). This indicates a potential micro-fracture or pinhole leak that allowed the xenon fission gas to escape. With ^{133}Xe ($t_{½}$ = 5.25 d) having a significantly longer half-life relative to the ^{135}Xe ($t_{½}$ = 9.14 h) and ^{137}Xe ($t_{½}$ = 3.82 m), the 24 h post-irradiation breach resulted in the loss of more ^{133}Xe and, in turn, lower levels of ^{133}Cs in the target leachate.

Table 16. The measured and ORIGEN-predicted atomic percent ratios for cesium at t=178 h, post-irradiation. The precision of the measurement is a 2σ standard deviation of the replicates. The origin model was modified to remove xenon and iodine fission products a t=24h post irradiation, which matches the observed atom % much more closely

Isotope	RAPID (meas. at. %) (2σ, n=3)	ORIGEN (calc. at. %)	ORIGEN (calc. at. %) with Xe release after 24 h
^{133}Cs	**14.8(2)**	22.7	13.98
^{135}Cs	**35.5(6)**	38.7	35.77
^{137}Cs	**49.7(8)**	38.6	50.22

Table 17 shows another way to view the data: isotope ratios as a function of time. With two isotopes growing in and one decaying away during the experiment, the neodymium isotope ratios are a good example of how closely the RAPID method can match extremely low-level (~80 fg of ^{144}Nd was injected onto the column in the first analysis) isotope ratios with multiple potential isobaric interferences.

Table 17. The measured and ORIGEN-predicted atomic percent ratios for neodymium at t=178 h, 504 h, and 1018 h post-irradiation. The precision of the measurement is a 2σ standard deviation of the replicates

Time Post Irradiation (h)	178		504		1018	
Isotope Ratio	RAPID (meas. at. %) (2σ, n=3)	ORIGEN (calc. at. %)	RAPID (meas. at. %) (2σ, n=3)	ORIGEN (calc. at. %)	RAPID (meas. at. %) (2σ, n=3)	ORIGEN (calc. at. %)
^{143}Nd/^{146}Nd ↑	0.46(2)	0.48	1.23(3)	1.25	1.70(4)	1.74
^{144}Nd/^{146}Nd ↑	0.038(4)	0.033	0.12(3)	0.093	0.18(3)	0.18
^{145}Nd/^{146}Nd –	1.36(6)	1.31	1.322(8)	1.31	1.33(3)	1.31
^{147}Nd/^{146}Nd ↓	0.47(2)	0.47	0.19(6)	0.19	0.051(6)	0.051
^{148}Nd/^{146}Nd –	0.56(3)	0.56	0.58(4)	0.56	0.57(1)	0.56
^{150}Nd/^{146}Nd –	0.24(2)	0.22	0.22(3)	0.22	0.22(1)	0.22

↓↑– represent decaying, ingrowing, and static numerator respectively.

Two masses of particular interest were 143 and 147 as, over the six-week period of analysis, quantitative shifts in the ^{143}Ce/^{143}Pr/^{143}Nd and ^{147}Nd/^{147}Pm/^{147}Sm abundances were observed (see **Figure 13**). These measurements were fitted with an exponential decay curve, and the half-lives of ^{147}Nd and ^{143}Pr were calculated as 10.6(3) d and 13.9(4) d respectively ($t_{1/2}$ ^{147}Nd = 10.98 d, $t_{1/2}$ ^{143}Pr = 13.57 d [65]). This was only possible due to the baseline resolution of the neighboring isotopes. To correct for day-to-day systematic, bias-inducing, variations in an ICPMS, normalization of the isotope signals was performed using a stable isotope standard within each run.

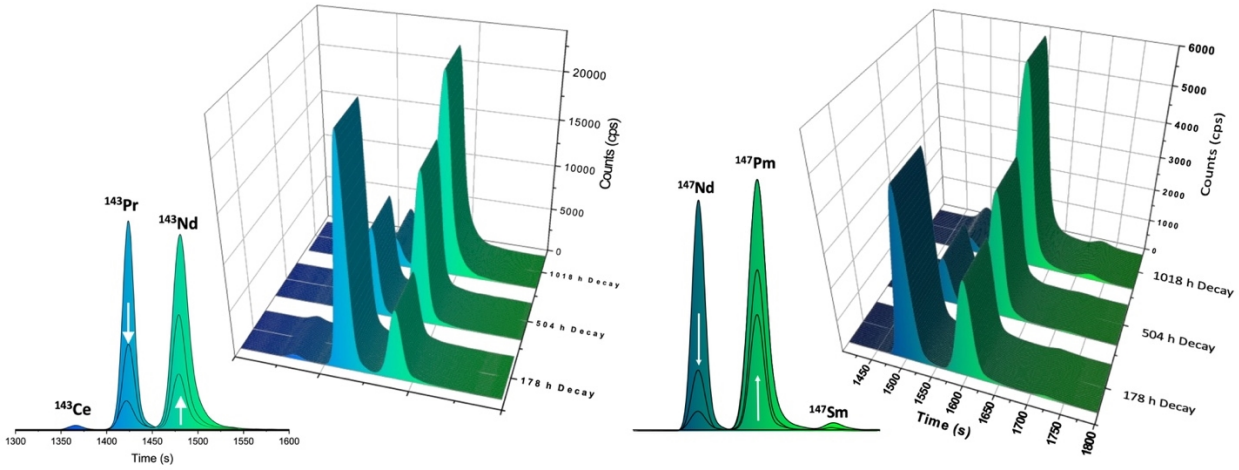

Figure 13. The transient ICPMS signals for m/z 143 (left) and 147 (right) for a 50 µL injection of the irradiated target leachates at 178 h, 504 h, and 1018 h post-irradiation. The figure depicts the transient signals separated by time, showing a clear separation between the isobars ^{143}Ce/^{143}Pr/^{143}Nd and ^{147}Nd/^{147}Pm/^{147}Sm. When a staggered plot of the transient signals is plotted by analysis time post-irradiation, the decay and ingrowth of the isobars can be observed.

4.3 ADDITIONAL LEACHATE ANALYSES

IDMS of the target leachate using a NIST-traceable, certified, ^{238}U standard (IV-ICPMS-71A, Inorganic Ventures) yielded a uranium recovery of 98(3) percent, with the main source of uncertainty being the verified initial mass of the loaded uranium target. The target was then analyzed for fission content using the RAPID determined isotopic compositions for each of the fission elements and NIST-traceable multi-element standards. The elemental concentrations in the irradiated target leachate were determined using both the RAPID online analysis and offline ICPMS analysis (utilizing a traditional linear regression external calibration for masses without pre-determined isobaric interferences). Both analyses agreed within 2–5% for all analytes, however, when compared to the ORIGEN-predicted values, the elemental recoveries were only ~55–60 percent. **Figure 14** shows the offline (red square) and online (black circle) results determined for each isotope mass (isotopes of the same mass were summed) in the target and compared with that predicted by ORIGEN (blue dotted line). These data sets were overlaid on an offline ICPMS mass spectrum scan, which further illustrates the utility of separation before analysis; without it, no differentiation can be made between isobars, and other interfering factors such as Xe, Kr, and doubly-charged ^{235}U (all noted in **Figure 14**). There were a number of analytes that can be measured offline but were either too low to detect via online analysis, or do not elute with the current HPIC separation protocol, namely molybdenum and technetium.

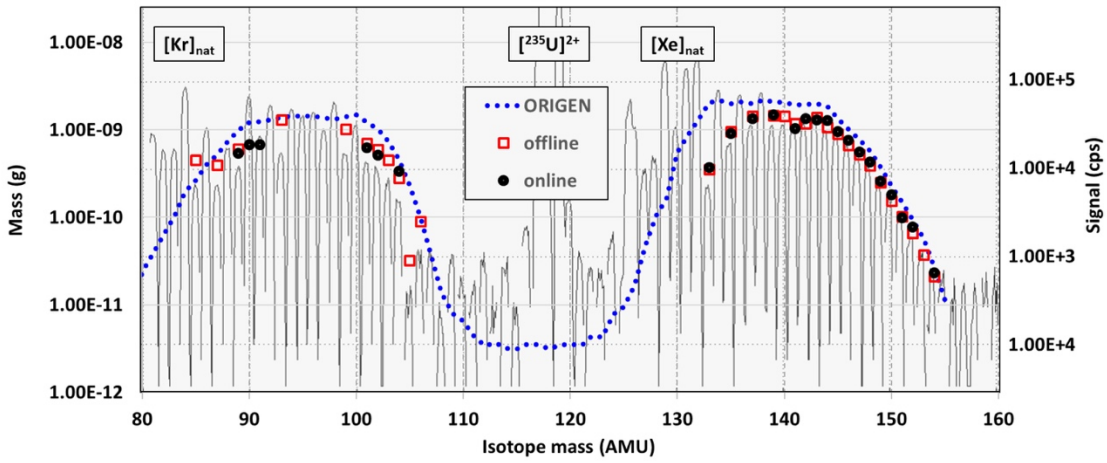

Figure 14. A plot displaying the offline (red square) and online (black circle) analysis for each isotope mass (isotopes of the same mass were summed) in the target, compared with that predicted by ORIGEN (blue dotted line). The right y-axis is for the mass spectrum scan (gray lines) and the left y-axis is for the measured and predicted concentration data.

Lastly, gamma spectra of the irradiated pellet leachate were acquired using an HPGe detector. A number of fission isotopes were observed (see supplementary information), six of which were measured using both methods at 178 h with very good agreement. **Table 18** shows the total amount of each of the fission isotopes in the irradiated pellet measured through both gamma analysis and RAPID. The recoveries of these isotopes in particular, when compared to gamma analysis, demonstrates the efficiency of the separation scheme, as all of these species have at least one isobaric interference when analyzed by mass.

Table 18. The concentrations of six short-lived isotopes determined using both gamma spectroscopy and the RAPID protocol

Analyte	Half-Life (d)	Gamma (ng total)	RAPID (ng total)	$mass_{gamma}/mass_{RAPID}$ (%)
^{140}La	1.68	0.107	0.108	99%
^{141}Ce	32.51	1.072	1.028	104%
^{143}Ce	1.38	0.024	0.023	105%
^{144}Ce	284.91	1.330	1.250	106%
^{147}Nd	10.98	0.338	0.345	98%
^{149}Pm	2.21	0.021	0.022	99%

It was hoped that the previous application of IDMS to RAPID for the acquisition of low-uncertainty measurements of lanthanide elements in a complex matrix [54] could be repeated here. However, it would only be warranted if full recovery of the sample was achieved. To understand this issue of low recovery, the SRIM software [61] was used to calculate the range of these fission isotopes, with an assumed 200 MeV energy (per fission), into a silicon target. It was calculated that, upon fission, the fission isotopes embed themselves ~20–25 μm into the walls of the quartz ampoule, making complete recovery via leaching difficult. A second, more aggressive, 8-hour heated leach with nitric (2ml, 8M, Optima) and hydrochloric acid (1 ml, 10M, Optima) yielded an additional 20% recovery, confirming that the primary leach was not aggressive enough and that the assumption of uranium recovery being equivalent to the fission product recoveries was incorrect. In order to completely recover the elemental concentrations of these fission products in future studies, a partial microwave-assisted digest of the ampoule will be required.

5. CONCLUSIONS

A rapid separation-direct analysis scheme to determine both concentration and isotopic composition of a suite of elements down to the low picogram level in less than 5 h has been developed. It has been shown that lanthanide element concentrations can rapidly be determined to as low as 1% uncertainty, without the need for offline separation or purification, via the use of isotope dilution. The developed method has flexibility to either focus on certain analytes for a lower uncertainty measurement, or to provide a quick screening method yielding concentrations for a multitude of elements in a short amount of time. There is potential for it to be applied to systems where trace analyses of impurities and fission products in nuclear materials is required. The reduced handling of the sample, when compared to traditional trace analysis techniques, will ensure that the method detection limits should be the limiting factor when analyzing sub-nanogram impurity levels in a solution.

Overall, acquisition of the concentration and isotopic composition of 48 elements in a single analysis has been developed. The method robustness to complex silicon-based matrices was proven over a 24 h period, yielding standard deviations of approximately 5%. The sensitivity of the analytical method appears to essentially be unaffected by a surrogate soil matrix, with most of the limits of detection maintained in the low picogram range. Application of the RAPID method, in combination with IDMS, to a NIST-certified Montana II soil standard (SRM2711a) showed that it is possible to spike, digest, analyze, and process the data for the isotopic composition and elemental concentration of five lanthanides in less than a 12 h period.

The duplicate analyses yielded results well within the uncertainties of the certificate values with the potential to drop the analysis time to less than 8 h if only one replicate is analyzed.

The work was then expanded further to show both the sensitivity and precision of the RAPID method when applied to elements of non-natural isotopic abundances in a uranium matrix. After leaching of the irradiated HEU targets, the isotopic compositions of several key fission elements, namely cesium, strontium, yttrium, lanthanum, cerium, praseodymium, neodymium, promethium, and samarium, were investigated. Fission isotopes with half-lives as short as 33 h were successfully measured by mass 178 h post-irradiation. The majority of the major isotopes of each element presented a 1–2% difference between measured and an ORIGEN model, even with some of the analyzed masses existing at the femtogram level. Elemental concentrations were also determined using both the RAPID method and an offline ICPMS linear regression external calibration. The isotopic concentrations of a number of short-lived isotopes were further confirmed by gamma analysis. Although the uranium in the target leachate was confirmed within 1% of the loaded material, the energetic nature of fission products resulted in partial recovery of the fission elements. This knowledge will lead to a more intensive digestion of future irradiated samples. Further investigations include the application of IDMS for high-precision fission isotopic concentration measurements and the application of the method to an irradiated ^{239}Pu-based material. Once the method has been established using well-characterized isotopes, we also plan on extending the application to lesser characterized and modeled isotopes, such as ^{237}Np, which is of interest at ORNL, as it is the target isotope used for the production of ^{238}Pu.

6. ACKNOWLEDGEMENT

This submission has been authored by a contractor of the U.S. Government under contract No. DE AC05-00OR22725. Accordingly, the U.S. Government retains a non-exclusive, royalty-free license to publish or reproduce the published form of this contribution, or allow others to do so, for the U.S. Government purposes. The authors of this work would like to acknowledge the Defense Threat Reduction Agency for funding.

7. REFERENCES

1. Hofmann S (2003) Chapter 1: Properties and Syntheses of Superheavy Elements. In: Schädel M (ed) The Chemistry of Superheavy Elements. Kluwer Academic Publishers, pp 1–27

2. Roberto JB, Alexander CW, Boll RA, et al (2015) Actinide targets for the synthesis of super-heavy elements. Nucl Phys A 944:99–116 . doi: 10.1016/j.nuclphysa.2015.06.009

3. Keegan E, Kristo MJ, Toole K, et al (2016) Nuclear Forensics: Scientific Analysis Supporting Law Enforcement and Nuclear Security Investigations. Anal Chem 88:1496–1505 . doi: 10.1021/acs.analchem.5b02915

4. Gauld IC, Giaquinto JM, Delashmitt JS, et al (2016) Re-evaluation of spent nuclear fuel assay data for the Three Mile Island unit 1 reactor and application to code validation. Ann Nucl Energy 87:267–281 . doi: 10.1016/j.anucene.2015.08.026

5. Ilas G, Gauld IC, Radulescu G (2012) Validation of new depletion capabilities and ENDF/B-VII data libraries in SCALE. Ann Nucl Energy 46:43–55 . doi: 10.1016/j.anucene.2012.03.012

6. Cantrel L, Cousin F, Bosland L, et al (2014) ASTEC V2 severe accident integral code: Fission product modelling and validation. Nucl Eng Des 272:195–206 . doi: 10.1016/j.nucengdes.2014.01.011

7. Tait JC, Gauld I, Kerr AH (1995) Validation of the ORIGEN-S code for predicting radionuclide inventories in used CANDU fuel. J Nucl Mater 223:109–121 . doi: 10.1016/0022-3115(94)00683-0

8. Casoli P, Authier N, Laurec J, et al (2012) Measurements of Actinide-Fission Product Yields in Caliban and Prospero Metallic Core Reactor Fission-Neutron Fields. J ASTM Int 9:104018 . doi: 10.1520/JAI104018

9. Chadwick MB, Kawano T, Barr DW, et al (2010) Fission Product Yields from Fission Spectrum n+239Pu for ENDF/B-VII.1. Nucl Data Sheets 111:2923–2964 . doi: 10.1016/j.nds.2010.11.003

10. Shinohara N, Kohno N, Nakahara Y, et al (2003) Validation of Minor Actinide Cross Sections by Studying Samples Irradiated for 492 Days at the Dounreay Prototype Fast Reactor—I: Radiochemical Analysis. Nucl Sci Eng 144:115–128 . doi: 10.13182/NSE03-A2347

11. Bolles RC, Ballou NE (1959) Calculated Activities and Abundances of U235 Fission Products. Nucl Sci Eng 5:156–185 . doi: 10.13182/NSE59-A25574

12. Tipnis S V., Campbell JM, Couchell GP, et al (1998) Yields of short-lived fission products produced following 235U thermal neutron fission. Phys Rev C 58:905–915 . doi: 10.1103/PhysRevC.58.905

13. Metz LA, Payne RF, Friese JI, et al (2009) Experimental measurements of short-lived fission products from uranium, neptunium, plutonium and americium. J Radioanal Nucl Chem 282:373–377 . doi: 10.1007/s10967-009-0225-1

14. Dayman K, Biegalski S, Haas D (2015) Determination of short-lived fission product yields with gamma spectrometry. J Radioanal Nucl Chem 305:213–223 . doi: 10.1007/s10967-015-3993-9

15. Finn EC, Metz L, Greenwood L, et al (2015) Cumulative fission yields of short-lived isotopes under natural-abundance-boron-carbide-moderated neutron spectrum. J Radioanal Nucl Chem 306:79–91 . doi: 10.1007/s10967-015-4085-6

16. Knowles J, Skutnik S, Glasgow D, Kapsimalis R (2016) A generalized method for characterization of 235U and 239Pu content using short-lived fission product gamma spectroscopy. Nucl Instruments Methods Phys Res Sect A Accel Spectrometers, Detect Assoc Equip 833:38–44 . doi: 10.1016/j.nima.2016.06.112

17. Tshiashala MDA (2005) Instrumental neutron activation analysis in geochemistry: Emphasis on spectral and uranium fission product interferences. J Radioanal Nucl Chem 265:511–514 . doi: 10.1007/s10967-005-0857-8

18. Landsberger S, Simsons A (1987) Quantification of uranium, thorium and gadolinium spectral interferences in instrumental neutron activation analysis of samarium. Chem Geol 62:223–226 . doi: 10.1016/0009-2541(87)90087-8

19. Bu W, Zheng J, Liu X, et al (2016) Mass spectrometry for the determination of fission products 135Cs, 137Cs and 90Sr: A review of methodology and applications. Spectrochim Acta Part B At Spectrosc 119:65–75 . doi: 10.1016/j.sab.2016.03.008

20. Almon AC, Kinard WF, Dewberry RA, et al (1991) Multimodal Separation of Alkali, Alkaline Earth, Transition, Post-Transition, Lanthanide, and Actinide Metal Cations in Waste Sludge (U).

In: Symposium for Ion Chromatography in the Power Industry. New Orleans, LA

21. Betti M (1997) Use of ion chromatography for the determination of fission products and actinides in nuclear applications. J Chromatogr A 789:369–379 . doi: 10.1016/S0021-9673(97)00784-X

22. Bruzzoniti MC, Cavalli S, Mangia A, et al (2003) Ion chromatography with inductively coupled plasma mass spectrometry, a powerful analytical tool for complex matrices Estimation of Pt and Pd in environmental samples. J Chromatogr A 997:51–63 . doi: 10.1016/S0021-9673(03)00547-8

23. Truscott J, Jones P, Fairman B, Evans E (2001) Determination of actinides in environmental and biological samples using high-performance chelation ion chromatography coupled to sector-field inductively coupled plasma mass spectrometry. J Chromatogr A 928:91–98 . doi: 10.1016/S0021-9673(01)01120-7

24. Epov V, Lariviere D, Reiber K, et al (2004) Extraction and determination of Cs in natural waters by ICP-MS after ion exchange separation. J Anal Atom Spectrom 19:1225–1229 . doi: 10.1039/B403013C

25. Betti M, Menichetti L, Moreno JM, Fuoco R (2000) A preliminary study for the determination of long-lived radionuclides (second transition group 4-d) in environmental samples by ion chromatography inductively coupled plasma-mass spectrometry (IC-ICP-MS). Microchem J 67:285–290 . doi: 10.1016/S0026-265X(00)00074-6

26. Röllin S, Kopatjtic Z, Wernli B, Magyar B (1996) Determination of Lanthanides and Actinides in Uranium Materials by High-Performance Liquid Chromatography with Inductively Coupled Plasma Mass Spectrometry. 739:139–149

27. Smith MR, Iii OTF, Reeves JH, Koppenaal DW (1995) Radionuclide detection by ion-chromatography and online ICPMS and beta detection: fission product rare earth elemtn measurements. J Radioanal Nucl Chem 194:7–13

28. Alonso JIG, Sena F, Arbore P, et al (1995) Determination of fission products and actinides in spent nuclear fuels by isotope dilution ion chromatography inductively coupled plasma mass spectrometry. J Anal At Spectrom 10:381 . doi: 10.1039/ja9951000381

29. Röllin S, Eklund UB, Spahiu K (2001) Separation of actinide redox species with cation exchange chromatography and its application to the analysis of spent fuel leaching solutions. Radiochim

Acta 89:757–763

30. Wolf SF, Bowers DL, Cunnane JC (2005) Analysis of high burnup spent nuclear fuel by ICP-MS. J Radioanal Nucl Chem 263:581–586

31. Snow M, Morrison S, Clark S, et al (2017) 237Np analytical method using 239Np tracers and application to a contaminated nuclear disposal facility. J Env Radioact 172:89–95 . doi: 10.1016/j.jenvrad.2017.02.018

32. Karasinski J, Bulska E, Wojciechowski M, et al (2017) High precision direct analysis of magnesium isotope ratio by ion chromatography/multicollector-ICPMS using wet and dry plasma conditions. Talanta 165:64–68 . doi: 10.1016/j.talanta.2016.12.033

33. Silvia G-R, Moldovan M, Alonso J (2007) Measurement of strontium isotope ratios by MC-ICP-MS after on-line Rb–Sr ion chromatography separation. J Anal Atom Spectrom 23:84–93 . doi: 10.1039/B708936H

34. Karasinski J, Bulska E, Wojciechowski M, et al (2016) On-line separation of strontium from a matrix and determination of the 87Sr/86Sr ratio by Ion Chromatography/Multicollector-ICPMS. J Anal At Spectrom 31:1459–1463 . doi: 10.1039/c6ja00109b

35. Yang G, Tazoe H, Yamada M (2016) Rapid determination of 135Cs and precise 135Cs/137Cs atomic ratio in environmental samples by single-column chromatography coupled to triple-quadrupole inductively coupled plasma-mass spectrometry. Anal Chim Acta 908:177–184 . doi: 10.1016/j.aca.2015.12.041

36. Liao H, Zheng J, Wu F, et al (2008) Determination of plutonium isotopes in freshwater lake sediments by sector-field ICP-MS after separation using ion-exchange chromatography. Appl Radiat Isot 66:1138–1145 . doi: 10.1016/j.apradiso.2008.01.001

37. Puzas A, Genys P, Remeikis V, Druteikienė R (2015) Challenges in preparing soil samples and performing a reliable plutonium isotopic analysis by ICP-MS. J Radioanal Nucl Ch 303:751–759 . doi: 10.1007/s10967-014-3411-8

38. Guéguen F, Isnard H, Nonell A, et al (2014) Neodymium isotope ratio measurements by {LC-MC-ICPMS} for nuclear applications: investigation of isotopic fractionation and mass bias correction. J Anal Atom Spectrom 30:443–452 . doi: 10.1039/C4JA00361F

39. Gourgiotis A, Isnard H, Nonell A, et al (2013) Bk and Cf chromatographic separation and 249Bk/248Cm and 249Cf/248Cm elemental ratios determination by inductively coupled plasma quadrupole mass spectrometry. Talanta 106:39–44 . doi: 10.1016/j.talanta.2012.11.056

40. Bourgeois M, Isnard H, Gourgiotis A, et al (2011) Sm isotope composition and Sm/Eu ratio determination in an irradiated 15 Eu sample by ion exchange chromatography -quadrupole inductively coupled plasma mass spectrometry combined with double spike isotope dilution technique. J Anal Atom Spectrom 26:1660–1666 . doi: 10.1039/C1JA10070J

41. Michalski R, Jablonska M, Szopa S, Łyko A (2011) Application of ion chromatography with ICP-MS or MS detection to the determination of selected halides and metal/metalloids species. Crit Rev Anal Chem 41:133–150 . doi: 10.1080/10408347.2011.559438

42. Winter C, Seubert A (2016) Usability of online-coupling ion exchange chromatography ICP-AES/-MS for the determination of trivalent metal complex species under acidic conditions. J Anal Atom Spectrom 31:1262–1268 . doi: 10.1039/C5JA00480B

43. Fassett JD, Paulsen PJ (1989) Isotope Dilution Mass Spectrometry for Accurate Elemental Analysis. Anal Chem 61:643–649 . doi: 10.1021/ac00185a001

44. Heumann KG (1992) Isotope dilution mass spectrometry (IDMS) of the elements. Mass Spectrom Rev 11:41–67 . doi: 10.1002/mas.1280110104

45. Vogl J (2007) Characterisation of Reference Materials by Isotope Dilution Mass Spectrometry. 22: . doi: 10.1039/b614612k

46. Hu J, Giaquinto JM, Gauld IC, et al (2017) Analysis of new measurements of Calvert Cliffs spent fuel samples using SCALE 6.2. Ann Nucl Energy 106:221–234 . doi: 10.1016/j.anucene.2017.04.005

47. Areva (2012) Summary Report on Post-irradiation Examinations of {MOX} Fuel

48. Eppich G, Knight K, Timothy J-H, et al (2014) Constraints on fallout melt glass formation from a near-surface nuclear test. J Radioanal Nucl Ch 302:593–609 . doi: 10.1007/s10967-014-3293-9

49. Hanson S, Pollington A, Waidmann C, et al (2016) Measurements of extinct fission products in nuclear bomb debris: Determination of the yield of the Trinity nuclear test 70 y later. Proc Natl

Acad Sci 113:8104–8108 . doi: 10.1073/pnas.1602792113

50. Ivanova J, Djingova R, Korhammer S, Markert B (2001) On the microwave digestion of soils and sediments for determination of lanthanides and some toxic and essential elements by inductively coupled plasma source mass spectrometry. Talanta 54:567–574 . doi: 10.1016/S0039-9140(00)00640-8

51. Reilly D, Ensslin N, Smith Jr H, Kreiner S (1991) Passive Nondestructive Assay of Nuclear Materials. United States Nuclear Regulatory Commission

52. Rearden BT (2018) Oak Ridge National Laboratory SCALE Website. https://www.ornl.gov/scale/overview

53. Gauld IC, Radulescu G, Ilas G, et al (2011) Isotopic Depletion and Decay Methods and Analysis Capabilities in SCALE. Nucl Technol 174:169–195 . doi: 10.13182/NT11-3

54. Roach BD, Fenske EK, Ilgner RH, et al (2018) Development of a fast and efficient analytical technique for the isotopic analysis of fission and actinide elements in environmental matrices. J Chromatogr A 1587:155–165 . doi: 10.1016/j.chroma.2018.12.029

55. Roach BD, Hexel CR, Giaquinto JM (2017) ORNL TM-2017-694: Demonstration of a Rapid HPLC-ICPMS Direct Coupling Technique Using IDMS Project Report Part I

56. Roach BD, Glasgow DC, Fenske EK, et al (2017) ORNL TM-2017-697: Demonstration of a Rapid HPLC-ICPMS Direct Coupling Technique Using IDMS Project Report Part II

57. FDA (2015) Analytical Procedures and Methods Validation for Drugs and Biologics. Guid Ind 1–15

58. IOS (2000) Capability of Detection - Part 2: Methodology in the Linear Calibration Case. International Organization for Standardization

59. IOS (1996) Linear Calibration Using Reference Materials. International Organization for Standardization

60. Thompson M, Ellison S, Wood R (2001) Harmonized Guidelines for Single Laboratory Validation of Methods of Analysis. 74:835–855

61. Ziegler JF, Ziegler MD, Biersack JP (2010) SRIM - The stopping and range of ions in matter (2010). Nucl Instruments Methods Phys Res Sect B Beam Interact with Mater Atoms 268:1818–1823 . doi: 10.1016/j.nimb.2010.02.091

62. Manuals (2002) Thermo Scientific - IC - Product Manual for Dionex IonPac™ CS5A and CS5G Manual

63. Dionex (2001) IonPac CS5A Column and MetPac Reagents

64. Dionex (1991) TN-23: Ion Chromatography of Lanthanide Metals

65. BNL National Nuclear Data Center. http://www.nndc.bnl.gov/

66. NIST (2018) Certificate of Analysis for SRM 2711a Montana Soil

67. Mackey EA, Lindstrom RM, Murphy KE (2010) Certification of Three NIST Renewal Soil Standard Reference Materials for Element Content

68. Rosman KJR, Taylor PDP (1998) Isotopic compositions of the elements 1997 (Technical Report). Pure Appl Chem 70:217–235 . doi: 10.1351/pac199870010217